Requirements for FisB-mediated membrane fission during sporulation

Ane Landajuela[1,2†*], Martha Braun[2,3†], Christopher D. A. Rodrigues[4], Thierry Doan[5], Florian Horenkamp[6#], Anna Andronicos[1‡], Vladimir Shteyn[1,2,] Nathan D. Williams[2,6], Chenxiang Lin[2,6], David Z. Rudner[7], Erdem Karatekin[1,2,3,8*]

1 Cellular and Molecular Physiology, Yale University, New Haven, CT, USA

2 Nanobiology Institute, Yale University, West Haven, CT, USA

3 Molecular Biophysics and Biochemistry, Yale University, New Haven, CT, USA

4 ithree Institute, University of Technology Sydney (UTS), Australia

5 Laboratoire d'Ingénierie des Systèmes Macromoléculaires, Aix-Marseille Université - CNRS UMR7255, Marseilles, France

6 Cell Biology, Yale University

7 Department of Microbiology, Harvard Medical School, Boston MA

8 Université de Paris, SPPIN - Saints-Pères Paris Institute for the Neurosciences, Centre National de la Recherche Scientifique (CNRS), F-75006 Paris, France.

† These authors contributed equally

Present address: Pfizer, New London, CT

‡ Present address: Department of Biological Chemistry, School of Medicine, U. California Irvine

* To whom correspondence should be addressed

ane.landajuela@yale.edu

erdem.karatekin@yale.edu (lead contact)

ABSTRACT

Little is known about mechanisms of membrane fission in bacteria despite their requirement for cytokinesis. The only known dedicated membrane fission machinery in bacteria, FisB, is expressed during sporulation in *Bacillus subtilis* and is required at the last stage of engulfment to release the developing spore into the mother cell cytoplasm. Here we characterize the requirements for FisB-mediated fission. FisB forms mobile clusters of ~12 molecules that give way to an immobile cluster at the engulfment pole containing ~40 proteins at the time of membrane fission. Reducing FisB to ~6 copies at the pole slowed but did not eliminate fission. Function mutants revealed that binding to acidic lipids and homo-oligomerization are both critical for targeting FisB to the engulfment pole and membrane fission. Finally, a distant FisB homolog from *Clostridium perfringens* was functional in *B. subtilis* suggesting FisB catalyzes fission without protein partners. Our results suggest that FisB is a robust and unusual membrane fission protein that likely relies on homo-oligomerization, lipid-binding and the unique membrane topology generated during engulfment for localization and membrane scission.

INTRODUCTION

Membrane fission is a fundamental process required for endocytosis (Haucke & Kozlov, 2018), membrane trafficking (Campelo & Malhotra, 2012), enveloped virus budding (Ahmed, Akram et al., 2019), phagocytosis (Jaumouille & Waterman, 2020), cell division (Carlton, Jones et al., 2020) and sporulation (Errington, 2003, Higgins & Dworkin, 2012, Tan & Ramamurthi, 2014). During membrane fission, an initially continuous membrane divides into two separate ones. This process requires dynamic localization of specialized proteins, which generate the work required to merge membranes (Bashkirov, Akimov et al., 2008, Kozlov, McMahon et al., 2010, Kozlovsky & Kozlov, 2003, Rand & Parsegian, 1986, Wong, Park et al., 1999). Dynamin (Ferguson & De Camilli, 2012) and the endosomal sorting complex required for transport III (ESCRT-III) catalyze many eukaryotic membrane fission reactions (Schoneberg, Lee et al., 2017). Both fission machineries bind acidic lipids, assemble into oligomers, and use hydrolysis of a nucleoside triphosphate (GTP or ATP) to achieve membrane fission. However, membrane fission can also be achieved by friction (Simunovic, Manneville et al., 2017), stress accumulated at a boundary between lipid domains (Roux, Cuvelier et al., 2005), forces generated by the acto-myosin network (Hatch, Gurel et al., 2014, Lacy, Ma et al., 2018, Nickaeen, Berro et al., 2019, Yang & Svitkina, 2019) or protein crowding (Snead, Zeno et al., 2019). By contrast, very little is known about membrane fission in bacteria, even though they rely on membrane fission for every division cycle.

We previously found that fission protein B (FisB) is required for the final membrane fission event during sporulation in *B. subtilis* (Doan, Coleman et al., 2013). When nutrients are scarce, bacteria in the orders *Bacillales* and *Clostridiales* initiate a developmental program that results in the production of highly resistant endospores (Stragier & Losick, 1996). Sporulation starts with an asymmetric cell division that generates a larger mother cell and a smaller forespore (Figure 1A). The mother cell membranes then engulf the forespore in a process similar to phagocytosis. At the end of engulfment, the leading membrane edge forms a small pore. Fission of this membrane neck connecting the engulfment membrane to the rest of the mother cell membrane releases the forespore, now surrounded by two membranes, into the mother cell cytoplasm (Figure 1A,B). Once the forespore has matured into a spore, the mother cell releases the spore into the environment through lysis. Spores can withstand heat, radiation, drought, antibiotics, and other environmental assaults for hundreds of years (Brown & Hovmøller, 2002, Cano & Borucki, 1995, Gest & Mandelstam, 1987, Potts, 1994). Under favorable conditions, the spore will germinate and restart the vegetative life cycle.

FisB is a transmembrane protein, conserved among endospore-forming bacteria, that is in the mother cell shortly after asymmetric division, upon activation of the transcription factor σ^E (Doan et al., 2013). In FisB knock-out cells, engulfment proceeds normally but the final membrane fission event, detected using a lipophilic dye, is impaired (Figure 1C,F and Fig. S1A). During engulfment, FisB fused to a fluorescent protein forms dim, mobile clusters in the engulfment membrane (Figure 1D,E, Movie S1). Around 3 hours into sporulation (t=3 h), a cluster of FisB molecules accumulates at the engulfment pole to form a more intense, immobile focus, where and when fission occurs (Figure 1D,E, Movie S2).

We had previously reported (Doan et al., 2013) that FisB interacts with cardiolipin (CL), a lipid enriched at cell poles (Kawai, Shoda et al., 2004, Koppelman, Den Blaauwen et al., 2001, Mileykovskaya & Dowhan, 2000) whose levels increase during sporulation (Kawai, Hara et al., 2006) and is implicated in membrane fusion (Haines, 2009, Lewis & McElhaney, 2009, Ortiz, Killian et al., 1999) and fission reactions (Khalifat, Puff et al., 2008). In addition, CL was reported to act as a landmark for the polar recruitment of the proline transporter ProP, and the mechanosensitive channel MscSm (Romantsov, Helbig et al., 2007, Romantsov, Stalker et al., 2008). Thus, it seemed plausible that CL could act as a landmark to recruit FisB to the membrane fission site and facilitate membrane fission. Apart from this hypothesis, no information has been available about how FisB localizes to the membrane fission site and how it may drive membrane scission.

Here, using a strategy that allowed us to monitor FisB dynamics and membrane fission simultaneously, we determined the requirements for FisB's sub-cellular localization and membrane fission during sporulation. Using quantitative analysis, we find small clusters of ~12 FisB molecules diffuse around the mother cell membrane and ~40 copies of FisB accumulate at the fission site into an immobile cluster to mediate membrane fission. When FisB expression was lowered, ~6 copies of FisB were sufficient to drive membrane fission, but fission took longer. Unexpectedly, FisB dynamics and membrane fission are independent of both CL and phosphatidylethanolamine (PE), another lipid implicated in membrane fusion and fission. We found FisB binds phosphatidylglycerol (PG) with comparable affinity as CL, after adjusting for charge density. Thus, we suspect that, as a more abundant lipid in the cell, PG can substitute for CL. We tested for other factors that may be important for the sub-cellular localization of FisB and membrane fission. We found FisB dynamics are also independent of flotillins which organize bacterial membranes into functional membrane microdomains (Lopez & Koch, 2017), cell wall synthesis machinery, and proton or voltage gradients across the membrane. Using mutagenesis, we show that both FisB oligomerization and binding to acidic lipids are required for proper localization and membrane fission. Together, these results suggest FisB-FisB and FisB-lipid interactions, and the unique membrane topology generated at the engulfment pole during sporulation alone, provide a simple mechanism to recruit FisB to mediate membrane fission independent of other factors. This idea is supported by complementation of *B. subtilis ΔfisB* cells by *C. perfringens* FisB, despite only ~23% identity between the two proteins.

RESULTS

Membrane fission always occurs in the presence of a cluster of FisB molecules

To correlate FisB dynamics with membrane fission, we devised a labeling strategy that allowed us to monitor both simultaneously, using a modified version of a fission assay developed previously (Sharp & Pogliano, 1999). In this assay, synchronous sporulation is induced by placing *B. subtilis* cells in a nutrient-poor medium. At different time points after the nutrient downshift, small aliquots are taken from the suspension, stained with the lipophilic membrane dye FM4-64, mounted on an agar pad, and imaged using fluorescence microscopy. The dye is virtually non-fluorescent in the medium, and it

cannot cross the cell membrane. Thus, before fission, FM4-64 labels the outer leaflet of both the mother cell and the forespore membranes. After fission, only the outer leaflet of the mother cell is labeled (Figure S1B). Because post-fission cells and cells that never entered sporulation are labeled in the same manner, in addition to FM4-64, a fluorescent protein is expressed in the forespore under the control of the forespore-specific transcription factor σ^F to distinguish between the two cell types (Meyer, Gutierrez et al., 2010). This makes it challenging to monitor FisB dynamics simultaneously, which requires a third channel. As an alternative, we used another lipophilic dye, TMA-DPH, that has partial access to internal membranes and can distinguish between pre- and post-fission stages without need for a forespore reporter (Doan et al., 2013) (Figure 1C). Using TMA-DPH as the fission reporter, we quantified the percentage of cells that have undergone fission as a function of time, for wild-type, *fisB* knock-out (*ΔfisB*, strain BDR1083, see Table S2 for strains used), and *ΔfisB* cells complemented with FisB fused to monomeric EGFP (mGFP-FisB, strain BAM003) as shown in Figure 1D and 1F. These kinetic measurements reproduced results obtained using FM4-64 (Doan et al., 2013). Thus, TMA-DPH can be used as a faithful reporter of membrane fission, leaving a second channel for monitoring dynamics of FisB fused to a fluorescent reporter.

In the experiments of Figure 1D and 1F, we simultaneously monitored dynamics of mGFP-FisB and membrane fission. We found that membrane fission (detected in the TMA-DPH channel) is always accompanied by an intense, immobile mGFP-FisB signal at the engulfment pole (Figure 1D, time= 3hr into sporulation). This intense spot at the engulfment pole (ISEP) is distinct from the dimmer, mobile clusters (DMC) that appear at earlier times elsewhere (Figure 1D). By 3 h into sporulation, around 70 % of the cells expressing mGFP-FisB at native levels had an ISEP (Figure 1G), a number that was close to the percentage of cells that had undergone fission by then (Figure 1F).

We also monitored membrane fission and mGFP-FisB signals in a strain with lower FisB expression (Doan et al., 2013). In this strain (BAL003), there was an initial delay in the fraction of cells that had undergone fission, but fission accelerated after t=3 h to reach near wild-type levels at around t=4h (Figure 1E,F). The fraction of cells with an ISEP followed a similar pattern (Figure 1G). When we plotted the fraction of cells that had undergone fission at a given time against the fraction of cells with an ISEP at that time, there was a very strong correlation (Figure 1H). We conclude that membrane fission occurs in the presence of a large immobile cluster of FisB molecules at the site of fission.

30-50 FisB molecules accumulate at the engulfment pole to mediate membrane fission

We asked how many copies of FisB are recruited to the engulfment pole at the time of membrane fission and how this number is affected when expression levels are altered. For this quantification, we used DNA-origami based fluorescence standards we recently developed (Williams, Landajuela et al., 2020). These standards consist of DNA rods (~410 nm long and 7 nm wide) labeled with AF647 at both ends and a controlled number of mEGFP molecules along the rod (Figure 2A).

DNA-origami standards carrying different mEGFP copies were imaged using widefield fluorescence microscopy (Figure 2B). For each type of rod, the average total fluorescence intensity of single-rods was computed and plotted against the number of mEGFP molecules per rod, generating the calibration curve in Figure 2D. We generated *B. subtilis* cells expressing mEGFP-FisB at native levels (BAL001) in a *ΔfisB* background so that images of these cells obtained under identical imaging conditions as for the calibration curve in Figure 2D could be used to compute mEGFP-FisB copy numbers. We imaged mEGFP-FisB cells at t=3 h after sporulation was induced. From these same images, we estimated the total fluorescence of dim, mobile clusters (DMC) and ISEP in *B. subtilis* cells as a sum of background-corrected pixel values (Figure 2C). Using the average values of these total intensities, we estimate ~40 copies at the ISEP, and ~12 per DMC from the calibration in Figure 2D. From the total intensity of cells (Fig. S2E), we also estimate there are ~1000 FisB molecules per cell.

Two independent approaches resulted in slightly different copy number estimates. First, we used *B. subtilis* calibration strains (Guiziou, Sauveplane et al., 2016) to relate the total cell fluorescence (sum of pixel values) to copy numbers of super-folder GFP (sfGFP). Cells expressing known copy numbers of sfGFP were imaged in wide-field fluorescence and the total intensity, corrected for background, was plotted against sfGFP copy number (Fig. S2**Figure 2**A,B). We then imaged cells expressing an equivalent number of-sfGFP (strain SG13) or mEGFP (strain BAL038) molecules and found the total fluorescence was 2.4±0.2-fold higher for sfGFP (Fig. S2C). Using this correction factor, the calibration for sfGFP was converted to a calibration for mEGFP, the label used for imaging FisB (Fig. S2D). We then computed the distribution of total cell fluorescence in *B. subtilis ΔfisB* cells expressing mEGFP-FisB (BAL001) at native levels at t=3 h into sporulation (Fig. S2E). We also estimated the total fluorescence of DMC and the ISEP as a fraction of total cellular fluorescence intensity (Fig. S2F). Together with the calibration of Fig. S2D, the means of these distributions allowed us to estimate ~1300 total FisB copies per cell, of which ~50 are located at the ISEP. The DMCs contain ~16 copies of FisB on average by this estimate.

Second, we used quantitative Western blotting (WB) to relate the total number of FisB molecules per cell to fluorescence intensity. Purified recombinant mYFP was used to calibrate the average number of mGFP-FisB molecules per cell using WB, using anti-GFP antibodies (Fig. S3). This average number per cell (~700) was then used to calculate mGFP-FisB copies at the ISEP (~30 copies) and DMC (~10 copies) from the fluorescence measurements in Fig. S2F, the fraction of total cellular fluorescence signal found at ISEP or DMC.

We tracked the DMC to estimate how rapidly they move. From the tracks, we calculated the MSD as a function of time (Figure 2E). The short-time diffusion coefficient estimated from the MSD is $D_{DMC} \approx 2.8 \times 10^3\ \mathrm{nm}^2/\mathrm{s}$ (95% confidence interval CI=$2.76 - 2.85 \times 10^3\ \mathrm{nm}^2/\mathrm{s}$). This value is comparable to the diffusivity of FloA and FloT clusters of ~100 nm with $D \approx 6.9 \times 10^3$ and 4.1×10^3 μm²/s, respectively (Donovan & Bramkamp, 2009). By comparison, ISEP have $D_{ISEP} \approx 28\ \mathrm{nm}^2/\mathrm{s}$ (CI=$22.9 - 33.1\ \mathrm{nm}^2/\mathrm{s}$), two orders of magnitude smaller.

We performed similar estimations of FisB copy numbers for the low expression strain (BAL004) (Fig. S4). We found ~160±66, 122±51, or 83±6 (±SD) copies per cell using *B. subtilis* standards, DNA-origami, or the quantitative WB methods, respectively. For the ISEP, we found 8±2, 6±2, or 5±3 (±SD) copies of mGFP-FisB using the three approaches, respectively (Table S1). About 6 % of the total mGFP-FisB signal accumulated in ISEP, close to the ~4% in the native-expression strain (Fig. S4E). The DMC were too dim to quantify reliably. Assuming DMCs to be ~3-fold dimmer than ISEP like in the native-expression strain, each DMC would contain 2-3 mGFP-FisB, just below our detection limit. Interestingly, lowering the total expression of FisB per cell ~8-fold resulted in a ~6-fold reduction in the average number of FisB molecules found at the membrane fission site. Thus, only ~6 copies of FisB are sufficient to mediate membrane fission, but after some delay (Figure 1E,F).

In summary, 30-50 FisB molecules accumulate at the fission site to mediate membrane fission. Only 3-4 DMCs need to reach the fission site to provide the necessary numbers. When FisB expression is lowered ~8-fold, ~6 FisB molecules accumulate at the engulfment pole to mediate membrane fission, but fission takes longer.

Localization of FisB is not coupled to cell wall remodeling, the protonmotive force, or the membrane potential

Next, we systematically investigated factors that could affect FisB dynamics and consequently membrane fission. The sub-cellular localization and motion of many cellular components depend on the cell-wall remodeling machinery (Carballido-Lopez & Formstone, 2007, Carballido-Lopez, Formstone et al., 2006, Ojkic, López-Garrido et al., 2016), the protonmotive force and the membrane potential (Strahl & Hamoen, 2010). We first tested if any of these influenced dynamics of FisB.

Cell wall synthesis and degradation drive engulfment during sporulation (Meyer et al., 2010, Ojkic et al., 2016). It was suggested that cell wall remodeling might also drive fission of the engulfing membrane at the end of engulfment. We wondered whether FisB dynamics could be coupled to cell wall remodeling. Since inhibition of cell wall synthesis leads to engulfment defects, we expressed mGFP-FisB from an inducible promoter during vegetative growth and investigated effects of inhibition of cell wall synthesis by fosfomycin on the motion of FisB clusters. As a control, we chose to image GFP-Mbl in parallel experiments. Mbl is an actin homologue that controls cell wall synthesis and cell shape (Shaevitz & Gitai, 2010). Mbl forms filaments that are associated with the cell membrane and rotate around the cell circumference together with enzymes required for cell wall synthesis (Garner, Bernard et al., 2011). Mbl filaments stop moving and eventually disassemble upon treatment with fosfomycin (Schirner, Eun et al., 2015) which inhibits the formation of N-acetylmuramic acid, a building block of the bacterial cell wall (Silver, 2017).

We imaged cells expressing either mGFP-FisB (BMB014) or GFP-Mbl (BDR2061) using total internal reflection fluorescence microscopy (TIRFM) in the absence and presence of fosfomycin (Fig. S5). Kymograph analysis and quantification of single-particle tracks

confirmed that GFP-Mbl spots stop moving upon fosfomycin treatment (Fig. S5A-F and Supplementary Information, Supplementary Methods). By contrast, motions of mGFP-FisB spots were independent of fosfomycin, indicating dynamics of FisB clusters are independent of the cell-wall synthesis machinery.

The protonmotive force (PMF) is important for the localization of proteins that are involved in maintaining cell shape, such as MreB and Mbl, or cell division (e.g. FtsZ/FtsA) (Strahl & Hamoen, 2010). We tested whether the localization of FisB depends on the PMF by imaging mGFP-FisB (BAM003) during sporulation in the absence and presence of carbonyl cyanide m-chlorophenyl hydrazone (CCCP), a proton-ionophore that dissipates the membrane PMF. We found that the localization of GFP-FisB at t=3 h into sporulation is not affected by the PMF unlike the localization of Mbl (Figure S5G).

Proteins whose localization depends on the PMF also require an intact membrane potential. To see if the membrane potential affected FisB dynamics, we imaged mGFP-FisB (BAM003) in the presence and absence of valinomycin, an antibiotic that functions as a potassium carrier that depletes the transmembrane electric potential component of the PMF. We found that GFP-Mbl mislocalizes in the presence of valinomycin, whereas the localization of FisB is not affected (Figure S5G).

Together, these results show that the dynamic movement of FisB is independent of cell wall remodeling, the PMF, and the membrane potential.

FisB localization and membrane fission are independent of cardiolipin, phosphatidylethanolamine and flotillins

Previously, we reported that the recombinant, purified extracytoplasmic domain (ECD, see Figure 4A) of FisB interacts with artificial lipid bilayers containing CL (Doan et al., 2013). Thus, it seemed plausible that FisB-CL interactions could be important for the subcellular localization of FisB and membrane fission. To test this hypothesis, we generated a strain (BAM234) that carries deletions of the three known CL synthase genes *ywnE (clsA)*, *ywjE (clsB)* and *ywiE (clsC)* (Kunst, Ogasawara et al., 1997) (Figure 3A). Thin layer chromatography profiles of lipid extracts from both wild type and the CL synthase-deficient strain (at t=3 hours after sporulation was initiated) indicate that the cardiolipin synthase-deficient strain did not contain detectable levels of CL (Figure 3B). Cells deficient in CL grew normally but had a reduction in sporulation efficiency as assayed by heat-resistant (20 min at 80˚ C) colony forming units (Table S2 and Figure S1D) (Kawai et al., 2006). A reduction in sporulation efficiency measured in this manner can be due to a defect at one or several steps during sporulation or germination. Importantly, the membrane fission time course of *ΔclsABC* cells was indistinguishable from those of wild-type cells (Figure 3C,D), indicating the defect in sporulation is downstream of membrane fission. In addition, mYFP-FisB localization and dynamics were similar in *ΔclsABC* (BAL037) and wild-type (BAL002) cells (Figure 3F-H). The fraction of cells that had an ISEP, and the intensity of the ISEP, reflecting the number of FisB molecules recruited to the membrane fission site, were indistinguishable for wild-type and *ΔclsABC* cells (Figure 3G,H). We conclude that CL is not required for the subcellular localization of FisB or membrane fission.

Next, we tested a potential role for phosphatidylethanolamine (PE) a lipid implicated in membrane fusion and fission (Chernomordik & Kozlov, 2008, Schmid & Frolov, 2011). Similar to CL, PE is a cone-shape phospholipid with a tendency to form non-bilayer structures (Schmid & Frolov, 2011) and PE microdomains accumulate in septal membrane during asymmetric division and the engulfment/forespore membranes at various stages during sporulation (Nishibori, Kusaka et al., 2005). To generate cells lacking PE (strain BAL031), we interfered with the lipid synthesis pathway in *B. subtilis* shown in Figure 3A by deleting the *pssA* gene which encodes the enzyme phosphatidylserine synthase that mediates the first step in PE synthesis. We confirmed the lack of PE in these cells using thin layer chromatography (Figure 3B). Kinetics of membrane fission during sporulation were identical in *ΔpssA* and wild-type cells (Figure 3D), indicating PE does not play a significant role in membrane fission.

PE and CL domains in *B. subtilis* membranes tend to occur in the same sub-cellular regions (Nishibori et al., 2005), raising the possibility that CL and PE may compensate for each other. To test whether removing both CL and PE affects fission, we generated a quadruple mutant (BAL030) lacking both CL and PE (Figure 3B), leaving PG as the major phospholipid component of the membrane. Surprisingly, the quadruple mutant underwent fission with indistinguishable kinetics compared to wild-type (Figure 3C,D). Thus, two lipids with negative spontaneous curvature and implicated in membrane fusion and fission reactions in diverse contexts have no significant role in membrane fission mediated by FisB during sporulation.

In addition to CL and PE microdomains, bacteria also organize many signal transduction cascades and protein-protein interactions into functional membrane microdomains (FMMs), loose analogs of lipid rafts found in eukaryotic cells (Lopez & Koch, 2017). The FMMs of *B. subtilis* are enriched in polyisoprenoid lipids and contain two different flotillin-like proteins, FloT and FloA that form mobile foci in the plasma membrane that recruit FMM-associated proteins to promote their interactions and oligomerization (Good, Zalatan et al., 2011, Langhorst, Reuter et al., 2005). FloT-deficient cells have a sporulation defect, but which sporulation stage is impaired is not known (Donovan & Bramkamp, 2009). We observed that *ΔfloA* (BAL035), but not *ΔfloT* (BAL036), cells are impaired in sporulation as assayed by heat-resistant colony forming units (Table S2, and Figure S1D). However, when we monitored engulfment and membrane fission during sporulation, we found engulfment proceeded normally and that *ΔfloA* cells underwent fission at the same rate as wild type cells (Figure 3D). Thus, the sporulation defect in *ΔfloA* cells lies downstream of engulfment and membrane fission. This was confirmed by blocking formation of FMMs during sporulation by addition of 50 μM zaragozic acid (López & Kolter, 2010) to the sporulation medium which had no effect on the localization of mGPF-FisB (Figure 3E).

Together, these results imply that FisB-mediated membrane fission that marks the end of engulfment during sporulation is insensitive to the negative-curvature lipids CL, PE, and to FloA/T-dependent lipid domains.

FisB binds to acidic lipids

It has been suggested that PG may substitute for CL as a binding partner for many

proteins (Oliver, Crooks et al., 2014, Sohlenkamp & Geiger, 2015). Accordingly, we wondered whether this may also be the case for FisB. Because removing PG is lethal in *B. subtilis* (Kobayashi, Ehrlich et al., 2003), we could not test this idea in cells, so we turned to biochemical characterization.

Before testing interactions between the soluble extracytoplasmic domain (ECD) of FisB and lipids, we first established the topology of FisB. Most, but not all, algorithms (Fig. S6) predict FisB to possess a single transmembrane domain (TMD) with a small N-terminal cytoplasmic domain and a larger (23-kDa) ECD, as depicted in Figure 4A. We confirmed this predicted topology by testing the accessibility of cysteine residues introduced into FisB at various positions to a membrane impermeable, biotinylated, sulfhydryl-reactive reagent, 3-(*N*-maleimidylpropionyl) biocytin (MPB) (Bogdanov, Heacock et al., 2010) (Fig. S7, Materials and Methods, and Supplementary Information). Our attempts to determine the structure of recombinant, purified FisB ECD were unsuccessful, but a computational model of FisB for residues 44 to 225, covering most of the ECD is available (Ovchinnikov, Park et al., 2017) and is shown in Figure 4B. The model predicts a curved ECD structure, with ~3 nm and ~5 nm for the inner and outer radii of curvatures. The overall topology of FisB, with the predicted ECD structure is depicted in Figure 4B.

We probed interactions of FisB ECD with PG using a liposome co-flotation assay, illustrated in Figure 4C. Purified recombinant FisB ECD (200 pmol) was incubated with liposomes (40 nmol) in a total volume of 100 µl for 1 hour at room temperature and subsequently layered at the bottom of an iodixanol discontinuous density gradient. Upon equilibrium ultracentrifugation, the lighter liposomes float up to the interface between the two lowest density layers together with bound protein, while unbound protein remains at the bottom. We collected fractions and determined the percentage of protein co-floated with liposomes using SDS-PAGE and densitometry, as shown in Figure 4D. We first determined that binding of FisB ECD to liposomes containing 45% CL was not dependent on pH or the divalent ion Ca^{2+} (Fig. S8F and S8G). By contrast, the fraction of liposome-bound protein decreased rapidly as the ionic strength increased (Fig. S8H). These results indicated binding was mainly electrostatic in nature.

At neutral pH, CL carries two negative charges, whereas PG and phosphatidylserine (PS), a lipid not normally found in *B. subtilis* (den Kamp, Redai et al., 1969) carry only a single negative charge. If binding is mediated mainly by electrostatic interactions and no specific affinity for one lipid species or another is present, then we reasoned that liposomes carrying PG or PS at two times the mole fraction of CL should bind the same amount of FisB ECD, since the surface charge density would be the same. Indeed, similar amounts of FisB ECD were bound to liposomes carrying 30% CL, 60% PG, or 60% PS (Figure 4E). FisB ECD did not bind neutral phosphatidylcholine PC liposomes (Doan et al., 2013).

To quantify the affinity of FisB ECD for CL vs PG, we then titrated liposomes containing 45 mole % CL or PG and measured binding of 100 nM FisB ECD (Figure 4F). In these experiments, we used iFluor555 labeled FisB ECD (iFluor555-FisB ECD) and detected liposome-bound protein using fluorescence rather than densitometry of SYPRO-stained gels, which extended sensitivity to much lower protein concentrations. The resulting titration curves were fit to $f_b = K[L]/(1 + K[L])$, where f_b is the bound fraction of

protein, $[L]$ is the total lipid concentration (assumed to be $\gg$ [protein bound]), and $K = 1/K_d$ the apparent association constant, and K_d is the apparent dissociation constant (Buser, Sigal et al., 1994). Best fit values for K_d were 1.0 μM for CL (95% confidence interval CI=0.7-2.1 μM) and 3.6 μM for PG, respectively (CI=2.8-5.0, Figure 4F,G).

Together, these results suggest that while FisB has higher affinity for CL than for PG, the higher affinity results mainly from the higher charge carried by CL. FisB does not bind CL with much specificity; at the same surface charge density, FisB ECD binds PG, or even PS which is not a *B. subtilis* lipid, with similar affinity. Thus, *in vivo* FisB is likely to bind CL as well as PG which is much more abundant.

Purified FisB ECD forms soluble oligomers

FisB forms clusters of various sizes in cells as described above (Figure 1, 2) and does not appear to have other protein interaction partners (Doan et al., 2013). Thus, homo-oligomerization of FisB may be important for its function. We explored oligomerization of recombinant, soluble FisB ECD. When FisB ECD bearing a hexa-histidine tag is expressed in *E. coli* and purified to homogeneity by affinity chromatography, samples analyzed by SDS-PAGE show multiple bands corresponding to different oligomeric states (Figure 5D and Figure S8B). Size-exclusion chromatography (SEC) analysis resolved the purified protein into predominant high molecular weight oligomeric structures eluting over a wide range of sizes, and low molecular weight peaks comprising minor components (Figure 5E and Figure S8C, top). The minor peak at ~23 kDa (18ml elution volume) corresponds to monomeric FisB ECD, whereas the peak at ~400 kDa (15ml) is FisB ECD that co-elutes with another protein, likely the 60 kDa chaperone GroEL, a common contaminant in recombinant proteins purified from *E. coli* (Figure S8D). To rule out potential artefacts caused by the hexa-histidine affinity tag, we also purified FisB ECD using a GST-tag, which yielded similar results. The SEC of high molecular weight peaks collected from the initial chromatogram did not show a redistribution when re-analyzed (Figure S8C, bottom), suggesting that once formed, the oligomeric structures are stable for an hour or longer.

We analyzed the high molecular-weight SEC fractions (peaks 1 and 2) using electron microscopy (EM) after negative staining. This analysis revealed rod-like structures quite homogeneous in size, ~50 nm long and ~10 nm wide (Figure 5F and Figure S8E). These structures displayed conformational flexibility, which precluded structural analysis using cryoEM, (and likely hampered our attempts to crystallize FisB ECD). We estimate every rod-like oligomer can accommodate ~40 copies of the predicted structure of $FisB^{44\text{-}225}$ shown in Figure 5B, similar to the number of FisB molecules recruited to the membrane fission site in cells (Figure 2).

A FisB mutant that is selectively impaired in homo-oligomerization

To determine whether self-oligomerization and lipid-binding interactions are important for FisB's function, we generated a series of mutants, characterized oligomerization and lipid-binding of the mutant proteins *in vitro*, and analyzed FisB localization dynamics and

membrane fission during sporulation *in vivo*.

We suspected self-oligomerization of FisB was at least partially due to hydrophobic interactions. Accordingly, we first mutated conserved residues G175, I176, I195 and I196 in a highly hydrophobic region of FisB ECD (Figure 5A,B), producing a quadruple mutant, G175A,I176S, I195T, I196S ($FisB^{GIII}$). These residues are on the surface of the predicted structure of FisB ECD (Figure 5C), so are not expected to interfere with folding. Purified $FisB^{GIII}$ ECD displayed reduced oligomerization when analyzed using SDS PAGE or size exclusion chromatography (Figure 5D,E). Though much reduced in amplitude, a broad, high molecular weight peak was still present in size exclusion chromatograms (Figure 5E). Negative-stain EM analysis of this fraction revealed oligomerization with less defined size and structure compared to wild type FisB ECD (Figure 5G).

To test whether lipid binding of the GIII mutant was affected, we used the co-flotation assay described above, except only two fractions were collected (Figure 5H,I). This analysis revealed that, despite being impaired in self-oligomerization, $FisB^{GIII}$ ECD has lipid binding properties similar to wild-type with a dissociation constant $K_d^{GIII} = 1.6$ μM (95% confidence interval CI=0.9-5.1 μM), indistinguishable from that of wild type FisB ECD^{WT} ($K_d^{wt} = 1.0\ \mu\mathrm{M}, \mathrm{CI} = 0.7 - 2.1\ \mu\mathrm{M}$, Figure 5J).

$FisB^{K168D,K170E}$ ($FisB^{KK}$) is selectively impaired in binding acidic lipids

To engineer lipid-binding mutants, we took advantage of our observation that FisB binding to anionic lipids is principally mediated through electrostatic interactions (Figure S8H). We generated a series of mutants in which we either neutralized or inverted up to four charges (Fig. S10A and Table S2). The ECD of a set of charge neutralization mutants were expressed in *E. coli*, purified and tested for lipid binding using the liposome co-floatation assay described above (Figure 4C). The largest reductions in lipid binding were observed when lysines in a region comprising residues 168-172 were neutralized. This region corresponds to a highly positively charged pocket in the predicted model of FisB 44-225 (Figure 5C).

A partially overlapping set of FisB mutants were expressed in a *ΔfisB* background and tested for sporulation efficiency by monitoring formation of heat-resistant colonies (Fig. S10B-E). Again, the strongest reductions in sporulation efficiency were found when lysines 168, 170 or 172 were mutated (Fig. S10D). We decided to characterize the K168D, K170E mutation in more detail, as it produced the strongest reduction in sporulation efficiency.

We purified the ECD of $FisB^{K168D,K170E}$ ($FisB^{KK}$) from *E. coli* and tested its binding to liposomes containing 45 mole % CL using the co-floatation assay (Figure 5H-J). The dissociation constant for $FisB^{KK}$-acidic lipid binding was $K_d^{KK} = 9.1$ μM (CI=6.5-15.3 μM), nearly 10-fold lower than that for wild-type FisB ECD ($K_d^{wt} = 1.0\ \mu\mathrm{M}, \mathrm{CI} = 0.7 - 2.1\ \mu\mathrm{M}$, Figure 5I,J). Importantly, formation of oligomers was not affected (Figure 5D).

Thus, $FisB^{KK}$ is specifically impaired in binding to acidic lipids.

FisB-lipid interactions and homo-oligomerization are important for targeting FisB to the fission site

Using the FisB mutants selectively impaired in binding to lipids or homo-oligomerization, we investigated whether these activities were important for FisB's function *in vivo*. To analyze FisB clustering and targeting to the fission site, we fused wild-type FisB and the two mutants to an N-terminal monomeric YFP (mYFP) and expressed the fusions at lower levels (

Figure **6**A). We induced these strains to sporulate and monitored FisB dynamics and membrane fission using the lipophilic dye TMA-DPH. Both the lipid-binding ($FisB^{KK}$) and the oligomerization mutant ($FisB^{GIII}$) were targeted to the cell membrane. This was not the case for most of the other mutants we tested (Figure S10E, red and cyan boxes and Table S2). At t=1.5 h after shifting the cells to the sporulation medium, mYFP-FisB signal was visible in all strains without any distinguishing features. At 2.5 h into sporulation, a subset of cells expressing the wild-type FisB fusion had undergone membrane fission and these cells had an ISEP. By contrast, membrane fission was not evident in either of the mutants. By 3 h into sporulation, 25% of WT FisB cells had undergone fission, always with an accompanying ISEP. In the lipid binding $FisB^{KK}$ mutant, only 8% of the sporulating cells had accomplished membrane fission, but those that did had an ISEP (

Figure **6**B). Membrane fission events and the accompanying bright mYFP-FisB spots were very rare (0.6%) in the oligomerization-deficient $FisB^{GIII}$ mutant.

The distribution of fluorescence intensities of the foci from low-expression WT and KK cells were indistinguishable (

Figure **6**C). Using the DNA-origami fluorescence intensity calibration (Figure 2), we estimate 6±2 copies of low-expression FisB WT or the KK mutant to have accumulated at the fission site. For the GIII mutant, there were not enough cells with an intense spot to perform a similar analysis.

From TMA-DPH labeling, we determined the fraction of cells that successfully completed fission as a function of time (

Figure **6**D). Oligomerization-deficient $FisB^{GIII}$ was not able to induce fission, whereas the lipid-binding mutant $FisB^{KK}$ had a partial, but severe defect (~50% reduction compared to wild-type). Importantly, both mutants were expressed at levels similar to the wild-type (Fig. S9), so the defects to form an ISEP and undergo membrane fission are not due to lower expression levels.

Together, these results suggest FisB-lipid and FisB-FisB interactions are both important for targeting FisB to the fission site.

C. perfringens FisB can substitute for *B. subtilis* FisB

So far, our results suggest FisB-FisB and FisB-acidic lipid interactions are the main drivers for targeting FisB to the membrane fission site. If no other partners are involved, FisB should be largely an independent fission module, i.e. FisB homologs from different sporulating bacteria should be able to substitute for one another at least partially, even if sequence homology is low outside the consensus region. To test this idea, we expressed *Clostridium perfringens* FisB ($FisB^{Cperf}$) in *B. subtilis* cells lacking FisB (BAL005). The sequence identity is only 23% between FisB sequences from these two species (Fig. S11). In the heat-kill assay, $FisB^{Cperf}$ fully rescued *B. subtilis ΔfisB* defects (Figure 7A). *C. perfringens* FisB fused to mEGFP (mEGFP-$FisB^{Cperf}$) had similar dynamics as $FisB^{Bsubti}$, forming DMCs at early times that gave way to an ISEP where membrane fission occurs (Figure 7B). Population kinetics of membrane fission were slower with $FisB^{Cperf}$ (Figure 7C), but every cell that underwent fission had an ISEP as for the wild type protein. The intensity distribution of mEGFP-$FisB^{Cperf}$ ISEP was shifted to smaller values compared to mEGFP-$FisB^{Bsubti}$ ISEP (Figure 7D). Since the average ISEP intensity for $FisB^{Bsubti}$ corresponds to ~40 copies (Figure 2), we deduce ~9 copies of $FisB^{Cperf}$ accumulate at ISEP at the time of membrane fission. At t=3 h into sporulation, the percentage of cells with an ISEP was lower for cells expressing mEGFP-$FisB^{Cperf}$ (Figure 7E).

In all conditions tested so far, only cells that had an intense FisB spot at the engulfment pole had undergone fission (Figure 2,3,6, and 7). When we plotted the percentage of cells having an ISEP against the percentage of cells that have undergone fission at t=3 h, we found a nearly perfect correlation (Figure 7F). $FisB^{Cperf}$ fit this pattern well, despite having a low sequence identity to $FisB^{Bsubti}$, supporting the idea that FisB is an independent membrane fission module that does not rely on specific protein-protein interactions for its localization and function.

DISCUSSION

Previously, we showed that FisB is required for the membrane fission event that marks the completion of engulfment of the forespore by the mother cell (Doan et al., 2013). Here, we found a cluster of FisB molecules is always present at the membrane fission site as evidenced by an intense fluorescent spot at the engulfment pole (ISEP) using fluorescently tagged FisB. The number of FisB molecules accumulated at the ISEP correlates well with the fraction of cells having undergone membrane fission at a given time point after induction of sporulation (Figure 1,7). In addition, the number of wild-type FisB molecules per ISEP correlates with the total number of FisB molecules per cell (Figure S4). Thus, the kinetics of membrane fission is determined by the accumulation of FisB molecules at the fission site. The number of wild-type FisB copies accumulated at the fission site, in turn, is determined by the total copies of FisB per cell. Thus, lowering FisB expression could slow membrane fission by slowing the accumulation of

FisB at the pole, or by reducing the number of FisB molecules driving fission after they are localized at the fission site. Currently, we cannot distinguish between the two possibilities, and both may be operating simultaneously.

How is FisB recruited to the fission site? Our results suggest FisB does not rely on existing landmarks, lipid microdomains, cell-wall remodeling machinery, or pH or voltage gradients across the cell membrane for its dynamic localization. In addition, we could not detect proteins interacting with FisB other than itself using an anti-GFP resin pulling on YFP-FisB (Doan et al., 2013). By contrast, we found two properties of FisB are critical for its localization, namely clustering and binding to acidic lipids. FisB forms various clusters in *B. subtilis* during sporulation. Similarly, purified recombinant FisB ECD forms soluble oligomers. A mutant deficient in oligomerization ($FisB^{GIII}$) was also deficient in accumulating at the membrane fission site in sporulating cells and in membrane fission. Another mutant ($FisB^{KK}$) deficient in binding to negatively charged lipids but retaining its ability to form oligomers, was impaired in accumulating at the engulfment pole. Together, these results suggest FisB-FisB and FisB-lipid interactions are key drivers for FisB clustering and accumulation at the membrane fission site.

Can FisB oligomerization and lipid binding be sufficient to accumulate an immobile cluster of FisB molecules at the engulfment pole? We speculate that the geometry of the neck connecting the engulfment membrane to the rest of the mother cell membrane may also be important, as this is the only region in the cell where a cluster of FisB molecules could be "trapped", i.e. once a cluster is formed inside the neck, it cannot diffuse away without breaking apart (Figure 8). This idea is supported by the fact that we do not observe any FisB accumulation at the leading edge of the engulfment membrane until a thin neck has formed at the end of engulfment.

The first FisB oligomers that appear during sporulation are dim, mobile clusters (DMCs), each containing about a dozen FisB molecules. Diffusion of DMCs appears to be Brownian on the 10-20 s time scale (Figure 2), though a rigorous analysis would require taking into account the geometry of the system. A DMC can diffuse a typical distance of ~1 μm in ~ 5 min ($D_{DMC} \approx 3 \times 10^{-3} \mu m^2/s$, Figure 2E). By comparison, engulfment in individual cells takes ~60 min on average (Ojkic et al., 2016). Though the engulfment time is much longer than the DMC diffusion time, the neck region, with an inner diameter of several nanometers, only forms at the very end of the engulfment process. Thus, ~40 FisB molecules could be recruited at the neck through diffusion-limited capture of a few DMCs. However, we could not image such capture events directly, and cannot rule out that FisB can also diffuse as monomers.

How many FisB molecules are needed for efficient membrane fission? In cells completely lacking FisB, ~5% of the cells undergo membrane fission by t=3 h, compared to ~80 % or ~30% for cells expressing FisB at native or ~8-fold reduced levels, respectively (Figure 1F). The former achieve fission with ~40 copies, while the latter with only ~6. Thus, FisB is not absolutely required for membrane fission, but it

makes it much more efficient, i.e. FisB catalyzes membrane fission. The variable stoichiometry suggests that FisB does not oligomerize into a specific quaternary structure with a definite stoichiometry. This appears to be a common property among proteins catalyzing membrane fusion and fission, such as SNAREs (Hernandez, Kreutzberger et al., 2014, Mostafavi, Thiyagarajan et al., 2017, Wu, Bello et al., 2017) or dynamin (Ferguson & De Camilli, 2012). The smallest clusters associated with membrane fission had ~6 FisB copies on average. This number is likely sufficient to form at least one ring inside the membrane neck that eventually undergoes fission. Given that fission can occur in the absence of FisB, it is likely that the FisB cluster cooperates with other cellular processes to produce stress on this membrane neck.

We found FisB dynamics and membrane fission are not affected by removal of CL, PE, or both. CL and PE are widely implicated in membrane fission and fusion reactions due to their tendency to form non-bilayer structures (Chernomordik & Kozlov, 2008, Chernomordik, Kozlov et al., 1985, Cullis, de Kruijff et al., 1986, Landajuela, Hervás et al., 2016, Stepanyants, Macdonald et al., 2015). The fact that CL or PE do not affect membrane fission during sporulation is remarkable, because such lipids usually affect the kinetics and/or the extent of fusion/fission reactions even if they are not absolutely required (Chernomordik et al., 1985). We tested the role of CL in a strain that lacked all three known CL synthases, with no detectable CL levels. A previous study reported that in *ΔclsABC B. subtilis* cells, CL levels increase from undetectable during vegetative growth to readily detectable during sporulation (Kawai et al., 2004), suggesting a yet unidentified sporulation-specific CL synthase may exist. Our results differ from those of Kawai et al. in that we were unable to detect any CL in *ΔclsABC B. subtilis* cells during vegetative growth or sporulation. We suggest the differences may be due to the different strains used (Zeigler, Pragai et al., 2008), PY79 (Youngman, Perkins et al., 1983) here vs. BS168 (Spizizen, 1958) in Kawai et al..

Overall, our results suggest FisB localizes to the membrane fission site using only lipid-binding, homo-oligomerization, and likely the unique geometry encountered at the end of engulfment. We propose that accumulation of a high enough density of FisB leads to membrane fission, possibly by generating increased stress in the FisB network-membrane composite, or in cooperation with another cellular process. A FisB homologue with low sequence identity rescued fission defects in *ΔfisB B. subtilis* cells, consistent with the idea that FisB acts as an independent module relying solely on homo-oligomerization, lipid-binding, and sporulation geometry.

MATERIALS AND METHODS

Materials

E. coli cardiolipin (CL), *E. coli* L-α-phosphatidylglycerol (PG), egg L-α-phosphatidylcholine (eggPC), *E.coli* L-α-phosphatidylethanolamine (PE), 1,2-dioleoyl-

sn-glycero-3-phosphoethanolamine-N-(7-nitro-2-1,3-benzoxadiazol-4-yl) (NBD-PE), 1,2-dioleoyl-sn-glycero-3-phosphoethanolamine (DOPE), 1,2-dioleoyl-sn-glycero-3-phosphocholine (DOPC), 1,2-dioleoyl-sn-glycero-3-phospho-L-serine (DOPS) were purchased from Avanti Polar Lipids. 1-(4-Trimethylammoniumphenyl)-6-Phenyl-1,3,5-Hexatriene *p*-Toluenesulfonate (TMA-DPH) and *N*-(3-Triethylammoniumpropyl)-4-(6-(4-(Diethylamino) Phenyl) Hexatrienyl) Pyridinium Dibromide (FM4-64) were from Thermo Fisher Scientific. Molybdenum Blue spray reagent was from Sigma-Aldrich. Carbonyl cyanide m-chlorophenyl hydrazone (CCCP) was purchased from Abcam and valinomycin was purchased from VWR. 3-(N-maleimidylpropionyl)biocytin (MBP) was obtained from Invitrogen and the HRP-conjugated antibody from eBioscience. Zaragozic acid was purchased from Sigma-Aldrich. 4-acetamido-4′-maleimidylstilbene-2,2′-disulfonic acid (AMS) and zaragozic acid were from obtained from Cayman Chemical Company.

General *B. subtilis* methods

B. subtilis strains were derived from the prototrophic strain PY79 (Youngman et al., 1983). Sporulation was induced in liquid medium at 37°C by nutrient exhaustion in supplemented DS medium (DSM) (Schaeffer, Millet et al., 1965) or by resuspension according to the method of Sterlini & Mandelstam (Sterlini & Mandelstam, 1969). Sporulation efficiency was determined in 24–30 h cultures as the total number of heat-resistant (80°C for 20 min) colony forming units (CFUs) compared to wild-type heat-resistant CFUs. Lipid synthesis mutants were from the *Bacillus* knock-out (BKE) collection (Koo, Kritikos et al., 2017) and all were back-crossed twice into *B. subtilis* PY79 before assaying and prior to antibiotic cassette removal. Antibiotic cassette removal was performed using the temperature-sensitive plasmid pDR244 that constitutively expresses Cre recombinase (Koo et al., 2017). Cassette removal was further confirmed by PCR with primers flanking the deletion. *B. subtilis* strains were constructed using plasmidic or genomic DNA and a 1-step competence method. Site directed mutagenesis was performed using Agilent's Quick-change Lightning kit following manufacturer's instructions and mutations were confirmed by sequencing. The strains and plasmids used in this study are listed in Tables S2 and S3, respectively.

Live-cell fluorescence microscopy of *B. subtilis*

Cells were mounted on a 2% agarose pad containing resuspension medium using a gene frame (Bio-Rad). Cells were concentrated by centrifugation (3300g for 30 s) prior to mounting and visualization. This step had no impact on the localization of the fusion proteins. Fluorescence microscopy was performed using a Leica DMi8 wide-field inverted microscope equipped with an HC PL APO 100×DIC objective (NA=1.40) and an iXon Ultra 888 EMCCD Camera from Andor Technology. Membranes were stained with TMA-DPH at a final concentration of 100 µM. Excitation light intensity was set to 50% and exposure times were 300 ms for TMA-DPH (λ_{ex}=395/25 nm; λ_{em}=460/50 nm); 500 ms for m(E)GFP (λ_{ex}=470/40; λ_{em}=500-550) and 1 s for mYFP (λ_{ex}=510/25; λ_{em}>530) respectively. Images were acquired with Leica Application Suite X (LAS X) and analysis and processing were performed using the ImageJ software.

Determination of FisB's topology

We used the substituted cysteine accessibility method (SCAM, (Bogdanov, Zhang et al.,

2005)) to determine the topology of FisB. We first generated stains expressing FisB versions with a single cysteine substitution at position G6, L137, or A245, in a *ΔfisB* background. FisB does not have any endogenous cysteines. These point mutations decreased the sporulation efficiency slightly (Table S2), we assume without affecting the topology. We selectively biotinylated extra- or intracellular cysteines of *B. subtilis* protoplasts, produced by addition of 0.5 mg/ml lysozyme and incubating cells at 37°C for 1h with gentle rocking. Protoplasts were then incubated with the membrane-impermeant reagent 3-(N-maleimidylpropionyl)biocytin (MBP). To selectively label extracellular cysteines, protoplasts of sporulating cells at 2.5 h into sporulation were incubated with 100 µM MPB. The reaction was quenched with 50 mM DTT before cells were lysed with hypotonic shock. To label intracellular cysteines selectively, extracellular cysteines of protoplasts were first blocked AMS before cells were lysed and incubated with 100 µM MPB. The reaction was quenched by addition of 100 µM MPB. FisB was pulled down from the cell lysates as described in (Bogdanov et al., 2005) using an anti-Myc antibody (mAb #2276) and biotinylated proteins were detected by Western Blot using a HRP-conjugated-Avidin antibody. Further details are provided in the Supplementary Information, Supplementary Materials and Methods.

Expression, purification, and labeling of recombinant FisB protein

FisB ECD was purified as described in (Doan et al., 2013) but with slight modifications. Briefly, His_6-FisB ECD was expressed in *E. coli* BL21 (DE3) from New England Biolabs and purified using HisPur™ Ni-NTA Resin from Thermo Fisher Scientific. Protein expression was induced with 1 mM IPTG at OD_{600} = 0.6 overnight at 16°C. Cells were harvested by centrifugation and the pellet was resuspended in Lysis Buffer (20 mM HEPES, 500 mM NaCl, 0.5 mM TCEP, 20 mM Imidazole, 2% glycerol, 20 mM $MgCl_2$) and flash-frozen in liquid nitrogen. Pellets were thawed on ice and cells were lysed by 5 passes through a high-pressure homogenizer (Avestin EmulsiFlex-C3). The lysate was spun down at 100,000×g and the soluble fraction was incubated with HisPur™ Ni-NTA Resin for 2.5 h at 4°C while rotating. The bound protein was washed with Lysis Buffer, Lysis Buffer containing 50 mM and finally 100 mM Imidazole. The protein was eluted in Elution Buffer (20 mM HEPES, 500 mM NaCl, 0.5 mM TCEP, 200 mM Imidazole, 2% glycerol, 20 mM MgCl2). The protein was concentrated using a Vivaspin centrifugal concentrator with a 10 kDa molecular weight cutoff and the concentration determined by Bradford protein assay. The protein was stored at -80ºC.

In experiments with labeled FisB ECD, we used a cysteine mutation, G123C (FisB ECD does not have any endogenous cysteines). After expression and purification as above, iFluor555-maleimide (AAT Bioquest) was reacted with FisB ECD^{G123C} following the manufacturer's instructions. G123 is in a loop that if removed does not interfere with FisB's function (Figure S10).

Analytical size-exclusion chromatography (SEC) and negative-stain electron microscopy (EM)

For SEC analysis His_6-FisB ECD was loaded onto a Superose 6 Increase 10/300 GL column (GE) previously equilibrated with 20 mM HEPES, pH 7.5, 500 mM NaCl, 0.5 mM TCEP, 2% glycerol, 20 mM $MgCl_2$, running at a flow rate of 0.5 ml/min at 4ºC. The column was calibrated with Bio-Rad's Gel Filtration Standards. For negative stain EM

analysis, 4 µL of the indicated elution fractions were applied to 200-mesh copper grids coated with ~10 nm amorphous carbon film, negatively stained with 2% (wt/vol) uranyl acetate, and air-dried. Images were collected on a FEI Tecnai T12 microscope, with a LaB6 filament operating at 120 kV, and equipped with a Gatan CCD camera.

Inhibition of cell wall synthesis and analyses of FisB motions

Overnight cultures of GFP-Mbl (BDR2061) or IPTG-induced mGFP-FisB (BMB014) were diluted in CH medium to OD600 = 0.05. Expression of GFP-FisB was induced with 1 mM IPTG for 2h at 37°C. Expression of GFP-Mbl was induced with 10 mM xylose for 30 min when BDR2061 reached OD600 = 0.5. For imaging untreated cells, 1 ml of cells was washed twice with 1 ml PBS and finally resuspended in 10 µl PBS. 2 µl of cell suspension was spread on a 2% PBS agar pad for imaging. To inhibit cell-wall synthesis 50 µg/ml fosfomycin was added to the cultures 45 min before imaging. 1 ml of cells was washed twice with PBS containing 50 µg/ml fosfomycin and mounted on a PBS agar pad also containing fosfomycin. Cells were imaged using a Olympus IX81 microscope with a home-built polarized TIRF setup (Nikolaus & Karatekin, 2016). Exposure times were 50 ms for BDR2061 and 100 ms for BMB014. Movies were acquired at 1 frame/s. Movies collected for BMB014 were corrected for bleaching using the Bleaching Correction function (exponential method) in ImageJ. Kymographs were created with imageJ along the indicated axes. GFP fusion proteins were tracked using the ImageJ plugin TrackMate (Tinevez, Perry et al., 2017). A Laplacian of Gaussian (LoG) filter was used to detect particles with an estimated blob diameter 400 µm. Particles were tracked using the Simple LAP tracker with a 0.25 µm maximum linking distance and no frame gaps. MATLAB (Mathworks, Natick, MA) was used for further processing of the tracks. Mean squared displacement (MSD) was calculated using the MATLAB class @msdanalyzer (Tarantino, Tinevez et al., 2014).

The asymmetry of individual tracks was calculated as described in (Huet, Karatekin et al., 2006) using:

$$Asym = -log\left(1 - \frac{(R_1^2 - R_2^2)^2}{(R_1^2 + R_2^2)^2}\right)$$

where R_1 and R_2 are the principal components of the radius of gyration, equal to the square roots of the eigenvalues of the radius of gyration tensor $\boldsymbol{R_g}$:

$$\boldsymbol{R_g(i,j)} = \langle \boldsymbol{x_i x_j} \rangle - \langle \boldsymbol{x_i} \rangle \langle \boldsymbol{x_j} \rangle.$$

Tracking fluorescently-labeled FisB spots and estimation of diffusion coefficients

For estimating the mobility of DMC and ISEP, time-lapse movies were recorded with a frame rate of 1 s using wide-field microscopy (50% LED intensity, 300 ms exposure time, gain 300). Spot positions were tracked using SpeckleTrackerJ (Smith, Karatekin et al., 2011), a plugin for the image analysis software ImageJ (Schneider, Rasband et al., 2012). Mean-squared displacements (MSDs) were calculated using the MATLAB class @msdanalyzer (Tarantino et al., 2014).

Dissipation of membrane potential

Cells were concentrated by centrifugation (3300xg for 30 s) and 100 μM CCCP or 30 μM valinomycin was added just prior to mounting cells onto a 2% PBS agar pad also containing 100 μM CCCP or 30 μM valinomycin.

Lipid extraction and thin-layer chromatography (TLC)

Lipids were extracted from *B. subtilis* cells at 3 h into sporulation according to the method of Lacombe and Lubochinsky (Lacombe & Lubochinsky, 1988). Lipid extracts were analyzed by TLC on silica gel plates in mixtures of chloroform:hexane:methanol: acetic acid (50:30:10:5). Phospholipids were detected with Molybdenum Blue Reagent (Sigma-Aldrich).

Liposome preparation

Small unilamellar vesicles (SUVs) were prepared by mixing 1 μmol of total lipids at desired ratios. A thin lipid film was created using a rotary evaporator (Buchi). Any remaining organic solvent was removed by placing the lipid film under high vacuum for 2h. The lipid film was hydrated with 1 ml of RB-EDTA buffer [25 mM HEPES at pH 7.4, 140 mM KCl, 1 mM EDTA, 0.2 mM tris(2-carboxyethyl) phosphine] by shaking using an Eppendorf Thermomix for >30 min. The lipid suspension was then frozen and thawed 7 times using liquid nitrogen and a 37°C water bath and subsequently extruded 21 times through a 100 nm pore size polycarbonate filter using a mini-extruder (Avanti). All SUVs contained 1% NBD-PE to determine the final lipid concentration.

Liposome-protein co-floatation

For initial experiments, 40 nmol total lipid was incubated with 200 pmol FisB ECD for 1h at room temperature in a total volume of 100 μl. 200 μl of 60% Optiprep (iodixanol, Sigma-Aldrich) was added to the sample creating a 40% Optiprep solution. The sample was then layered at the bottom of a 5 mm x 41 mm Beckman ultracentrifuge tube (#344090) and overlaid with 200 μl of 20% Optiprep and finally 150 μl of buffer (Figure 4 C). Liposome-bound proteins co-float to a light density, while unbound proteins pellet upon ultracentrifugation for 1.5 h at 48 krpm. Fractions were collected as shown in Figure 4C and the amount of recovered protein was determined by SDS-PAGE (Nu-PAPGE 12% Bis-tris gel, Thermo Fisher Scientific) stained with SYPRO™ Orange (Invitrogen).

Determination of binding constants

For determination of binding constants, the floatation protocol was slightly modified. Varying amounts of lipids were incubated with 100 nM iFluor555-ECD for 1 h at room temperature in a total volume of 100 μl. Density gradients were created as before using Optiprep, however only 2 fractions were collected (Figure 5H). The protein concentration in fraction A was too small to be quantified by SDS-PAGE. Therefore, the sample was concentrated by trichloroacetic acid (TCA) precipitation. Briefly, 50 μl of TCA was added to fraction A and incubated for 30 min at 4°C. The sample was spun at 14 krpm in an Eppendorf microfuge for 5 min. The pellet was washed twice with ice-cold acetone and subsequently dried for 10 min in a 95°C heating block. 10 μl of 2X SDS sample buffer was added to the dried pellet and the sample was boiled for 10 min at 95°C and loaded on a 12% bis-tris gel. The amount of recovered protein was determined by fluorescence intensity of the labeled FisB ECD band on the gel using a

Typhoon FLA 9500 (GE Healthcare). The dissociation constant K_d was determined following (Buser et al., 1994). Titration curves were fitted to:

$$f_b = \frac{K[L]}{1+K[L]}, \qquad (1)$$

where f_b is the fraction of bound protein and K the apparent association constant ($K = 1/K_d$). Eq. (1) assumes that the total lipid concentration $[L]$ is much larger than the concentration of bound protein, a condition satisfied in our experiments for $[L] > 10^{-7}$ M.

Image analysis

For the analysis shown in Figure 5B and Fig. S4A,B,C,E, we calculated the total intensity (sum ox pixel values) inside the cell contour (indicated in yellow in Figure 5A) using MicrobeJ (Ducret, Quardokus et al., 2016). Mean integrated auto-fluorescence (~1300 a.u) was calculated by analyzing in the same way an equivalent number of individual wild-type cells, imaged under identical conditions.

For the analyses shown in Figure 2 and Figure 5D, FisB foci were semi-automatically selected using SpeckleTrackerJ (Smith et al., 2011). For each spot the sum of pixel values in a 6 × 6 pixel (0.5 μm × 0.5 μm) box around the center of the spot were calculated. For each corresponding cell the same operation was performed at a membrane area where no clusters were present and subtracted from the FisB cluster intensity.

Preparation of DNA Origami-based mEGFP standards

These standards were prepared and characterized as described in (Williams et al., 2020). Briefly, DNA "rods" consisted of six-helix-bundle DNA origami nanotubes. Rods carried varying numbers of single stranded “handle” sequences for DNA-conjugated fluorophore hybridization. A long scaffold DNA (p7308, (Douglas, Dietz et al., 2009)) was folded into the desired shape by self-assembly with a six-fold molar excess of designed "staple strands" by heating and cooling cycles over an 18-hour period in a thermocycler (Bio-Rad). Excess staples were removed by PEG precipitation (Stahl, Martin et al., 2014), and DNA-conjugated fluorophores were hybridized to the DNA origami nanotubes by coincubation for 2 hours at 37ºC. Finally, excess fluorophore-DNA conjugates were removed by a second PEG precipitation (Stahl et al., 2014). To estimate fluorophore labeling efficiency, standards designed to host 5 copies of Alexa Fluor 488 were similarly prepared. These standards were imaged on a TIRF microscope (Eclipse Ti, Nikon) until fully bleached. The photobleaching steps of the fluorescence traces were fit to a binomial function to estimate the labeling efficiency to be ~80% (95% CI = 76%-84%).

Quantitative Western Blot

mYFP was cloned into pVS001 (His_6-Sumo-mYFP) and purified using affinity chromatography. For immunoblotting, cells in 100 ml sporulation medium were pelleted and the supernatant removed. The pellets were suspended in ice-cold lysis buffer

(pH=7.5; 50 mM HEPES, 100 mM KCl, 3 mM $MgCl_2$, 1 mM EGTA, 0.1% Triton X-100, 1 mM DTT, 1 mM PMSF, with one complete protease inhibitor tablet (Roche) to a final volume of 300 µl, and then we added 0.3 g acid-washed glass beads (425-600 µm, Sigma). After adding 150 µl boiling sample buffer (250 mM Tris-HCl, pH 6.8, 50% glycerol, 3.58 µM β-mercaptoethanol, 15% SDS, and 0.025% Bromophenol Blue), samples were incubated at 100°C for 5 min. Samples were centrifuged at 14,000 rpm in a desktop centrifuge at room temperature for 10 min and stored at -80°C. The blots were probed with peroxidase-conjugated anti-GFP antibody (ab13970). Images were scanned and quantified using ImageJ.

ACKNOWLEDGEMENTS

We thank members of the Karatekin and Rudner laboratories for stimulating discussions. This work was supported by National Institute of General Medical Sciences and National Institute of Neurological Disorders and Stroke of the National Institutes of Health (NIH) under award numbers R01GM114513 and R01NS113236 (to EK), DP2GM114830 and R01GM132114 (to CL). The content is solely the responsibility of the authors and does not necessarily represent the official views of the National Institutes of Health. We thank Vladimir Polejaev and Jeorg Nikolaus (directors of the Yale West Campus Imaging Core), and Josh Lees (Yale Center for Cellular and Molecular Imaging Electron Microscopy Facility) for their help with imaging, Karin Reinisch in whose laboratory work by FH was carried out, Daniel R. Zeigler (Bacillus Genetic Stock Center) for helpful advice, and Alexander J. Meeske for some of the strains used in this study. NDW was supported by a NIH training grant (T32-EB09941). We gratefully acknowledge a Yale University Predoctoral Fellowship to MB.

AUTHOR CONTRIBUTIONS

AL, MB, VS, and EK conceived the study. AL and MB performed experiments whose results are shown in the main figures. AA (Fig. S10), FH (Fig. 5, 7, S8), VS (Fig. S3) performed additional experiments. NDW and CL developed the DNA-origami fluorescence calibration method and contributed to the data in Fig. 2. CR, TD, and DR provided resources, training, and technical and conceptual input. They introduced EK, AL, MB and VS to *B. subtilis* and sporulation. EK and DR provided supervision and acquired funding. AL, MB, and EK and wrote the manuscript, with input from other co-authors.

CONFLICT OF INTEREST

None.

FIGURE LEGENDS

Figure 1. Membrane fission during sporulation is always accompanied by accumulation of a FisB cluster at the fission site. **A**. Vegetatively growing cells enter sporulation when nutrients become scarce. Asymmetric division creates a forespore (FS) and a mother cell (MC). The MC engulfs the FC in a phagocytosis-like event. At the end of engulfment, a membrane neck connects the engulfment membrane to the rest of the MC (i). Fission of the neck (ii) releases the FS, now surrounded by two membranes, into the MC cytoplasm. Once the forespore becomes a mature spore, the MC lyses to release it. **B**. The membrane fission step shown in more detail. **C**. Detection of membrane fission. The lipophilic dye TMA-DPH does not fluoresce in the aqueous solution and crosses membranes poorly. If membrane fission has not yet taken place, the dye has access to the engulfment, FS and MC membranes, thus shows intense labeling where these membranes are adjacent to one another (i). If fission has already taken place, the dye labels internal membranes poorly (ii). **D.** Images show mGFP-FisB (strain BAM003, native expression level) at indicated times during sporulation. Membranes were visualized with TMA-DPH. Examples of sporulating cells with mGFP-FisB enriched at the septum (1.5h), forming dim mobile cluster (DMC; 2 h) and with a discrete mGFP-FisB focus at the cell pole (intense spot at engulfment pole, ISEP, 3 h) are highlighted with white arrowheads and magnified in the insets. **E.** Similar to D, but using a strain (BAL003) that expresses mGFP-FisB at lower levels in a *ΔfisB* background. **F.** Time course of membrane fission for wild-type cells, *ΔfisB* cells, or *ΔfisB* cells complemented with mGFP-FisB expressed at native (BAM003) or low levels (BAL003). Lower expression of mGFP-FisB leads to a delay in membrane fission kinetics. **G.** The percentage of cells with an intense spot at the engulfment pole (ISEP) for low and native level expression of mGFP-FisB as a function of time into sporulation. **H**. Correlation between percentage of cells that have undergone fission and percentage of cells having an ISEP for all time points shown in F and G. Scale bars represent 1 μm.

Figure 2. Estimation of mEGFP-FisB copies at the engulfment pole at t=3 h using DNA-origami calibration standards and mobility of FisB clusters. **A.** Simplified schematic of the DNA-origami-based mEGFP standards used in this study. Using DNA origami, DNA rods bearing AF647 at both ends and the indicated numbers of mEGFP molecules along the rod were designed. In the actual rods, the labeling efficiency was found to be ~80%, so the actual copies of mEGFP per rod were 4, 20, 40, 56, and 80. **B.** Representative wide field images of the DNA-origami-based mEGFP standards used in this study. Bars are 1 μm. **C**. Distributions of total fluorescence intensities (sum of pixel values) for the intense spot at the engulfment pole (ISEP) and the dim, mobile clusters (DMC). Background was defined for every cell where an ISEP or DMC intensity measurement was performed. Examples are shown on the left. **D.** Total fluorescence intensity (sum of pixel values) for DNA-origami rods as a function of mEGFP copy numbers. The best fit line passing through the origin has slope 29.56 au/mEGFP ($R^2 = 0.97$). The total intensity of the ISEP and DMCs correspond to ~40 and ~12 copies of mEGFP respectively. **E.** Mean-squared displacement (MSD) as a function of delay time for DMCs (magenta) and ISEPs (blue). Fits to the initial 25 s (~10 % of delays) yielded $D_{DMC} = 2.80 \pm 0.05 \times 10^3\ \mathrm{nm}^2/\mathrm{s}$ (± 95% confidence interval, $R^2 = 0.999$, 24 tracks) and

$D_{ISEP} = 2.80 \pm 0.51 \times 10$ nm^2/s (± 95% confidence interval, R^2 = 0.850, 25 tracks). **F.** Summary of FisB copy number and cluster mobility estimation.

Figure 3. Membrane fission is insensitive to membrane lipid composition. **A.** Pathways for membrane lipid synthesis in *B. subtilis*. Lipid synthetases responsible for each step are highlighted in blue. **B.** Thin-layer chromatography (TLC) of the total lipid extracts of wild-type and indicated lipid synthesis-deficient cells. Phospholipid spots (PLs) were visualized by staining with Molybdenum Blue spray reagent. Purified CL, PG, and PE were used as standards to identify the PLs of *B. subtilis*. Arrows indicate locations to which individual standards migrate. **C.** Membranes from cells of the indicated genetic backgrounds were visualized with TMA-DPH at t=3h. The images are from cells mounted on agarose pads containing sporulation medium. Bar,1 µm. **D.** Percentage of cells from indicated strains that have undergone membrane fission as a function of time after initiation of sporulation. **E.** mGFP-FisB (strain BAM003) treated with the squalene-synthase inhibitor zaragozic acid, imaged at t=3 h. **F.** Cells expressing mYFP-FisB (low expression levels) in either wild type (BAL002) or in a CL deficient strain (BAL037) at t=3h. Membranes were visualized with the fluorescent dye TMA-DPH. Examples of sporulating cells with a discrete mYFP-FisB focus at the cell pole (ISEP) are highlighted (white arrows). Foci were semi-automatically selected with SpeckletrackerJ (Smith et al., 2011). **G.** The percentage of cells with an intense spot at engulfment pole for wild-type (BAL002) or cardiolipin-deficient (BAL037) mYFP-FisB expressing cells at t=3h (low expression). **H.** Distributions of total fluorescence intensities (sum of pixel values) at ISEP for wild-type (BAL002) or cardiolipin-deficient (BAL037) mYFP-FisB cells at 3hr into sporulation. Scale bars are 1 µm.

Figure 4. **Binding of FisB ECD to acidic lipids. A**. Domain structure of FisB and its His_6-tagged extracytoplasmic domain (ECD) used in floatation experiments. **B.** Predicted model of $FisB^{44-225}$ comprising most of the ECD (Ovchinnikov et al., 2017), schematically attached to the membrane. **C**. Schematic of the floatation assay. Liposomes (40 nmol total lipid) and FisB ECD (200 pmol) were incubated for 1 hour at room temperature and layered at the bottom of an iodixanol density gradient. Upon ultracentrifugation, liposomes float to the top interface, whereas unbound protein remains at the bottom. Four fractions were collected as indicated and analyzed by SDS-PAGE. **D**. SYPRO orange stained gel of FisB ECD incubated with liposomes containing 45 mole % CL. The percentage of recovered protein is determined by comparing the intensity of the band in fraction B to the input band intensity. **E**. Indistinguishable amounts of FisB ECD are recovered when FisB ECD is incubated with liposomes containing different acidic lipid species as long as the charge density is similar. CL30, PG60, PS60 indicate liposomes containing 30 mole % CL, 60 mole % PG and 60 mole % PS, respectively. CL carries 2 negative charges, whereas PG and PS carry one each. The rest of the liposome composition is PC. **F**. Fraction of liposome-bound iFluor555-labeled FisB ECD (iFluor555-FisB ECD) recovered after floatation as a function of lipid concentration. Titration curves were fit to $f_b = K[L]/(1 + K[L])$, where f_b is the bound fraction of protein, $[L]$ is the total lipid concentration (assumed to be $\gg$ [protein bound]), and $K = 1/K_d$ the apparent association constant, and K_d is the apparent dissociation constant. **G**. Best fit values for K_d were 1.0 µM for CL (95% confidence interval, CI=0.7-2.1 µM) and 3.6 µM for PG (CI=2.8-5.0 µM), respectively. iFluor555-FisB ECD (100 nM)

was incubated with10^{-8} to 10^{-4} M lipids for 1 h at room temperature before flotation. Liposomes contained 45 mole % of CL or PG and 55% PC.

Figure 5. FisB mutants selectively impaired in oligomerization and membrane binding. A. Mutated residues shown on the FisB domain structure. **B**. Kyle-Doolittle hydrophobicity profile of the FisB sequence for wild-type (WT), FisB K168D,K170E ($FisB^{KK}$), and FisB G175A,I176S, I195T, I196S ($FisB^{GIII}$) mutants. **C.** Mutations shown on the predicted model of $FisB^{44-225}$ (Ovchinnikov et al., 2017). Residue conservation (top) and electrostatic potential (bottom) are mapped onto the structure. **D**. Western blot of cell lysates from *E. coli* cells expressing FisB-ECD^{WT}, FisB-ECD^{GIII}, or FisB-ECD^{KK}, probed with an anti-histidine antibody. High molecular weight bands in the WT and KK lanes are largely absent in the GIII lane, indicating $FisB^{GIII}$ is less prone to forming oligomers. **E**. Size-exclusion chromatography of FisB WT and the GIII mutant. Intensities of high and low molecular weight peaks are reversed for FisB WT and the GIII mutant. **F**. A fraction corresponding to the high-molecular peak in E (indicated by *) for FisB WT was collected and imaged using negative-stain electron microscopy (EM), which revealed flexible, elongated structures ~50 nm × 10 nm. **G**. A similar analysis for $FisB^{GIII}$ revealed more heterogeneous and less stable structures. Scale bars in F, G are 50 nm. **H**. Schematic of the floatation experiments to determine the apparent affinity of FisB mutants for liposomes containing acidic lipids. Experiments and analyses were carried out as in Figure 4, except only two fractions were collected. iFluor555-FisB ECD (100 nM) was incubated with10^{-8} to 10^{-4} M lipids for 1 h at room temperature before floatation. Liposomes contained 45 mole % of CL and 55% PC. **I**. Fraction of protein bound to liposomes as a function of total lipid concentration. Data was fitted to a model as in Figure 4F. The data and fit for FisB WT is copied from Figure 4F for comparison. **J.** Best fit values for K_d were 1.0 μM for WT (95% confidence interval, CI=0.7-2.1 μM), 9.1 μM for KK (CI=6.5-15.3 μM), and 1.6 for GIII (CI=0.9-5.1 μM), respectively**.**

Figure 6. FisB clustering and binding to acidic lipids are both required for ISEP formation and membrane fission. A. Snapshots of sporulating *ΔfisB* cells expressing mYPF-$FisB^{WT}$ (BAL002), mYPF-$FisB^{KK}$ (BAL006), or mYPF-$FisB^{GIII}$ (BAL007), at low levels. For each time point after downshifting to the sporulation medium, cell membranes were labeled with TMA-DPH and images were taken both in the membrane (left) and the YFP (right) channels. By t=2.5 h, some foci at the engulfment pole (ISEP) are visible for WT cells that have undergone membrane fission (red boxes), but not for the KK or GIII mutants (white boxes). A small fraction of KK mutants accumulated FisB at the engulfment pole and underwent membrane fission at t=3h. Scale bars represent 1 μm. **B.** Percentage of cells with an intense spot at the engulfment membrane (ISEP) at t=3 h into sporulation, for WT FisB, $FisB^{KK}$, or $FisB^{GIII}$. **C**. Distribution of background-corrected integrated intensities (sum of pixel values) of ISEP fluorescence for *ΔfisB* cells expressing mYFP-$FisB^{WT}$ or mYPF-$FisB^{KK}$. The distributions are indistinguishable. Since low-expression cells accumulate, on average, 6±2 $FisB^{WT}$ molecules at the ISEP (Fig. S4D), so do $FisB^{KK}$ cells. **D**. Percentage of cells that have undergone membrane fission at the indicated time points.

Figure 7. *C. perfringens* FisB can substitute for *B. subtilis* FisB despite poor sequence identity. A. Heat-resistant colony forming units for *ΔfisB* cells expressing *B. subtilis* (BAL001) or *C.perfringens* FisB (BAL005) at native levels, presented as a

percentage of the WT sporulation efficiency. Results are shown as means ± SD for three replicates per condition. **B.** Snapshot of *ΔfisB* cells expressing mEGFP-FisB^{Cperfringens}. Aliquots were removed at the indicated times, membranes labeled with TMA-DPH, and both the TMA-DPH and the EGFP channels imaged after mounting into agar pads. White boxed areas are shown on an expanded scale in yellow boxes. Arrows indicate cells with ISEP that have undergone membrane fission. Bar, 1 μm. **C**. Percentage of cells that have undergone membrane fission as a function of sporulation time for wild-type cells, *ΔfisB* cells, *ΔfisB* cells expressing *B. subtilis* mEGFP-FisB at native levels, or *ΔfisB* cells expressing mEGFP-FisB^{Cperfringens}**.** The plots for the first three conditions are reproduced from Figure 1F for comparison. **D.** Distribution of background-corrected total fluorescence intensity of ISEP for *ΔfisB* cells expressing mEGFP-FisB^{Cperfringens} or mEGFP-FisB^{Bsubtilis} at native levels. From the calibration in Figure 2D, we estimate 9±7 FisB^{Cperfringens} per ISEP. The distribution for mEGFP-FisB^{Bsubtilis} is reproduced from Figure 2C for comparison. **E**. Percentage of cells with ISEP, for *ΔfisB* cells expressing mEGFP-FisB^{Cperfringens} or mEGFP-FisB^{Bsubtilis}. **F**. Percentage of cells that have undergone membrane fission at t=3 h vs. the percentage of cells with ISEP at the same time point, for the conditions indicated. There is a nearly perfect correlation between these two quantities (the dashed line is a best-fit, $y = 1.03x, R^2 = 0.96$).

Figure 8. Summary of how FisB localizes to the engulfment pole. Left: Schematic of the late stages of engulfment, when a small fission pore connects the engulfment membrane to the rest of the mother cell membrane. Right: Schematic of FisB accumulation at the fission site. FisB freely moves around the engulfment membrane and other regions of the mother cell membrane in clusters of ~12 molecules. These motions are independent of lipid microdomains, flotillins, the cell-wall synthesis machinery, and voltage or pH gradients. About 40 copies of FisB accumulate at the fission site into an immobile cluster, possibly because leaving this region would require disruption of the cluster. We cannot exclude the presence of FisB monomers, which are below our detection limit (~3-4 mEGFP molecules).

REFERENCES

Ahmed I, Akram Z, Iqbal HMN, Munn AL (2019) The regulation of Endosomal Sorting Complex Required for Transport and accessory proteins in multivesicular body sorting and enveloped viral budding - An overview. *Int J Biol Macromol* 127: 1-11

Bashkirov PV, Akimov SA, Evseev AI, Schmid SL, Zimmerberg J, Frolov VA (2008) GTPase cycle of dynamin is coupled to membrane squeeze and release, leading to spontaneous fission. *Cell* 135: 1276-86

Bogdanov M, Heacock PN, Dowhan W (2010) Study of polytopic membrane protein topological organization as a function of membrane lipid composition. *Methods Mol Biol* 619: 79-101

Bogdanov M, Zhang W, Xie J, Dowhan W (2005) Transmembrane protein topology mapping by the substituted cysteine accessibility method (SCAM(TM)): application to lipid-specific membrane protein topogenesis. *Methods* 36: 148-71

Brown JK, Hovmøller MS (2002) Aerial dispersal of pathogens on the global and continental scales and its impact on plant disease. *Science* 297: 537-41

Buser CA, Sigal CT, Resh MD, McLaughlin S (1994) Membrane binding of myristylated peptides corresponding to the NH2 terminus of Src. *Biochemistry* 33: 13093-101

Campelo F, Malhotra V (2012) Membrane fission: the biogenesis of transport carriers. *Annu Rev Biochem* 81: 407-27

Cano RJ, Borucki MK (1995) Revival and identification of bacterial spores in 25- to 40-million-year-old Dominican amber. *Science* 268: 1060-4

Carballido-Lopez R, Formstone A (2007) Shape determination in Bacillus subtilis. *Curr Opin Microbiol* 10: 611-6

Carballido-Lopez R, Formstone A, Li Y, Ehrlich SD, Noirot P, Errington J (2006) Actin homolog MreBH governs cell morphogenesis by localization of the cell wall hydrolase LytE. *Dev Cell* 11: 399-409

Carlton JG, Jones H, Eggert US (2020) Membrane and organelle dynamics during cell division. *Nat Rev Mol Cell Biol* 21: 151-166

Chernomordik LV, Kozlov MM (2008) Mechanics of membrane fusion. *Nat Struct Mol Biol* 15: 675-83

Chernomordik LV, Kozlov MM, Melikyan GB, Abidor IG, Markin VS, Chizmadzhev YA (1985) The shape of lipid molecules and monolayer membrane fusion. *Biochimica et Biophysica Acta (BBA) - Biomembranes* 812: 643-655

Cullis PR, de Kruijff B, Verkleij AJ, Hope MJ (1986) Lipid polymorphism and membrane fusion. *Biochem Soc Trans* 14: 242-5

den Kamp JA, Redai I, van Deenen LL (1969) Phospholipid composition of Bacillus subtilis. *J Bacteriol* 99: 298-303

Doan T, Coleman J, Marquis KA, Meeske AJ, Burton BM, Karatekin E, Rudner DZ (2013) FisB mediates membrane fission during sporulation in Bacillus subtilis. *Genes Dev* 27: 322-34

Donovan C, Bramkamp M (2009) Characterization and subcellular localization of a bacterial flotillin homologue. *Microbiology* 155: 1786-1799

Douglas SM, Dietz H, Liedl T, Högberg B, Graf F, Shih WM (2009) Self-assembly of DNA into nanoscale three-dimensional shapes. *Nature* 459: 414-8

Ducret A, Quardokus EM, Brun YV (2016) MicrobeJ, a tool for high throughput bacterial cell detection and quantitative analysis. *Nat Microbiol* 1: 16077

Errington J (2003) Regulation of endospore formation in Bacillus subtilis. *Nat Rev Microbiol* 1: 117-26

Ferguson SM, De Camilli P (2012) Dynamin, a membrane-remodelling GTPase. *Nat Rev Mol Cell Biol* 13: 75-88

Garner EC, Bernard R, Wang W, Zhuang X, Rudner DZ, Mitchison T (2011) Coupled, circumferential motions of the cell wall synthesis machinery and MreB filaments in B. subtilis. *Science* 333: 222-5

Gest H, Mandelstam J (1987) Longevity of microorganisms in natural environments. *Microbiol Sci* 4: 69-71

Good MC, Zalatan JG, Lim WA (2011) Scaffold proteins: hubs for controlling the flow of cellular information. *Science* 332: 680-6

Guiziou S, Sauveplane V, Chang HJ, Clerté C, Declerck N, Jules M, Bonnet J (2016) A part toolbox to tune genetic expression in Bacillus subtilis. *Nucleic Acids Res* 44: 7495-508

Haines TH (2009) A new look at Cardiolipin. *Biochim Biophys Acta* 1788: 1997-2002

Hatch AL, Gurel PS, Higgs HN (2014) Novel roles for actin in mitochondrial fission. *J Cell Sci* 127: 4549-60

Haucke V, Kozlov MM (2018) Membrane remodeling in clathrin-mediated endocytosis. *J Cell Sci* 131

Hernandez JM, Kreutzberger AJ, Kiessling V, Tamm LK, Jahn R (2014) Variable cooperativity in SNARE-mediated membrane fusion. *Proc Natl Acad Sci U S A* 111: 12037-42

Higgins D, Dworkin J (2012) Recent progress in Bacillus subtilis sporulation. *FEMS Microbiol Rev* 36: 131-48

Huet S, Karatekin E, Tran VS, Fanget I, Cribier S, Henry JP (2006) Analysis of transient behavior in complex trajectories: application to secretory vesicle dynamics. *Biophys J* 91: 3542-59

Jaumouille V, Waterman CM (2020) Physical Constraints and Forces Involved in Phagocytosis. *Front Immunol* 11: 1097

Kawai F, Hara H, Takamatsu H, Watabe K, Matsumoto K (2006) Cardiolipin enrichment in spore membranes and its involvement in germination of Bacillus subtilis Marburg. *Genes Genet Syst* 81: 69-76

Kawai F, Shoda M, Harashima R, Sadaie Y, Hara H, Matsumoto K (2004) Cardiolipin domains in Bacillus subtilis marburg membranes. *J Bacteriol* 186: 1475-83

Khalifat N, Puff N, Bonneau S, Fournier JB, Angelova MI (2008) Membrane deformation under local pH gradient: mimicking mitochondrial cristae dynamics. *Biophys J* 95: 4924-33

Kobayashi K, Ehrlich SD, Albertini A, Amati G, Andersen KK, Arnaud M, Asai K, Ashikaga S, Aymerich S, Bessieres P, Boland F, Brignell SC, Bron S, Bunai K, Chapuis J, Christiansen LC, Danchin A, Debarbouille M, Dervyn E, Deuerling E et al. (2003) Essential Bacillus subtilis genes. *Proc Natl Acad Sci U S A* 100: 4678-83

Koo BM, Kritikos G, Farelli JD, Todor H, Tong K, Kimsey H, Wapinski I, Galardini M, Cabal A, Peters JM, Hachmann AB, Rudner DZ, Allen KN, Typas A, Gross CA (2017) Construction and Analysis of Two Genome-Scale Deletion Libraries for Bacillus subtilis. *Cell Syst* 4: 291-305.e7

Koppelman CM, Den Blaauwen T, Duursma MC, Heeren RM, Nanninga N (2001) Escherichia coli minicell membranes are enriched in cardiolipin. *J Bacteriol* 183: 6144-7

Kozlov MM, McMahon HT, Chernomordik LV (2010) Protein-driven membrane stresses in fusion and fission. *Trends Biochem Sci* 35: 699-706

Kozlovsky Y, Kozlov MM (2003) Membrane fission: model for intermediate structures. *Biophys J* 85: 85-96

Kunst F, Ogasawara N, Moszer I, Albertini AM, Alloni G, Azevedo V, Bertero MG, Bessieres P, Bolotin A, Borchert S, Borriss R, Boursier L, Brans A, Braun M, Brignell SC, Bron S, Brouillet S, Bruschi CV, Caldwell B, Capuano V et al. (1997) The complete genome sequence of the Gram-positive bacterium Bacillus subtilis. *Nature* 390: 249-256

Lacombe C, Lubochinsky B (1988) Specific extraction of bacterial cardiolipin from sporulating Bacillus subtilis. *Biochim Biophys Acta* 961: 183-7

Lacy MM, Ma R, Ravindra NG, Berro J (2018) Molecular mechanisms of force production in clathrin-mediated endocytosis. *FEBS Lett* 592: 3586-3605

Landajuela A, Hervás JH, Antón Z, Montes LR, Gil D, Valle M, Rodriguez JF, Goñi FM, Alonso A (2016) Lipid Geometry and Bilayer Curvature Modulate LC3/GABARAP-Mediated Model Autophagosomal Elongation. *Biophysical journal* 110: 411-422

Langhorst MF, Reuter A, Stuermer CA (2005) Scaffolding microdomains and beyond: the function of reggie/flotillin proteins. *Cell Mol Life Sci* 62: 2228-40

Lewis RN, McElhaney RN (2009) The physicochemical properties of cardiolipin bilayers and cardiolipin-containing lipid membranes. *Biochim Biophys Acta* 1788: 2069-79

Lopez D, Koch G (2017) Exploring functional membrane microdomains in bacteria: an overview. *Curr Opin Microbiol* 36: 76-84

López D, Kolter R (2010) Functional microdomains in bacterial membranes. *Genes Dev* 24: 1893-902

Meyer P, Gutierrez J, Pogliano K, Dworkin J (2010) Cell wall synthesis is necessary for membrane dynamics during sporulation of Bacillus subtilis. *Mol Microbiol* 76: 956-70

Mileykovskaya E, Dowhan W (2000) Visualization of phospholipid domains in Escherichia coli by using the cardiolipin-specific fluorescent dye 10-N-nonyl acridine orange. *J Bacteriol* 182: 1172-5

Mostafavi H, Thiyagarajan S, Stratton BS, Karatekin E, Warner JM, Rothman JE, O'Shaughnessy B (2017) Entropic forces drive self-organization and membrane fusion by SNARE proteins. *Proc Natl Acad Sci U S A* 114: 5455-5460

Nickaeen M, Berro J, Pollard TD, Slepchenko BM (2019) Actin assembly produces sufficient forces for endocytosis in yeast. *Mol Biol Cell* 30: 2014-2024

Nikolaus J, Karatekin E (2016) SNARE-mediated Fusion of Single Proteoliposomes with Tethered Supported Bilayers in a Microfluidic Flow Cell Monitored by Polarized TIRF Microscopy. *J Vis Exp*

Nishibori A, Kusaka J, Hara H, Umeda M, Matsumoto K (2005) Phosphatidylethanolamine Domains and Localization of Phospholipid Synthases in *Bacillus subtilis* Membranes. *Journal of Bacteriology* 187: 2163-2174

Ojkic N, López-Garrido J, Pogliano K, Endres RG (2016) Cell-wall remodeling drives engulfment during Bacillus subtilis sporulation. *Elife* 5

Oliver PM, Crooks JA, Leidl M, Yoon EJ, Saghatelian A, Weibel DB (2014) Localization of anionic phospholipids in Escherichia coli cells. *J Bacteriol* 196: 3386-98

Ortiz A, Killian JA, Verkleij AJ, Wilschut J (1999) Membrane fusion and the lamellar-to-inverted-hexagonal phase transition in cardiolipin vesicle systems induced by divalent cations. *Biophys J* 77: 2003-14

Ovchinnikov S, Park H, Varghese N, Huang PS, Pavlopoulos GA, Kim DE, Kamisetty H, Kyrpides NC, Baker D (2017) Protein structure determination using metagenome sequence data. *Science* 355: 294-298

Potts M (1994) Desiccation tolerance of prokaryotes. *Microbiol Rev* 58: 755-805

Rand RP, Parsegian VA (1986) Mimicry and mechanism in phospholipid models of membrane fusion. *Annu Rev Physiol* 48: 201-12

Romantsov T, Helbig S, Culham DE, Gill C, Stalker L, Wood JM (2007) Cardiolipin promotes polar localization of osmosensory transporter ProP in Escherichia coli. *Mol Microbiol* 64: 1455-65

Romantsov T, Stalker L, Culham DE, Wood JM (2008) Cardiolipin controls the osmotic stress response and the subcellular location of transporter ProP in Escherichia coli. *J Biol Chem* 283: 12314-23

Roux A, Cuvelier D, Nassoy P, Prost J, Bassereau P, Goud B (2005) Role of curvature and phase transition in lipid sorting and fission of membrane tubules. *EMBO J* 24: 1537-45

Schaeffer P, Millet J, Aubert JP (1965) Catabolic repression of bacterial sporulation. *Proc Natl Acad Sci U S A* 54: 704-11

Schirner K, Eun YJ, Dion M, Luo Y, Helmann JD, Garner EC, Walker S (2015) Lipid-linked cell wall precursors regulate membrane association of bacterial actin MreB. *Nat Chem Biol* 11: 38-45

Schmid SL, Frolov VA (2011) Dynamin: functional design of a membrane fission catalyst. *Annu Rev Cell Dev Biol* 27: 79-105

Schneider CA, Rasband WS, Eliceiri KW (2012) NIH Image to ImageJ: 25 years of image analysis. *Nat Methods* 9: 671-5

Schoneberg J, Lee IH, Iwasa JH, Hurley JH (2017) Reverse-topology membrane scission by the ESCRT proteins. *Nat Rev Mol Cell Biol* 18: 5-17

Shaevitz JW, Gitai Z (2010) The structure and function of bacterial actin homologs. *Cold Spring Harb Perspect Biol* 2: a000364

Sharp MD, Pogliano K (1999) An in vivo membrane fusion assay implicates SpoIIIE in the final stages of engulfment during Bacillus subtilis sporulation. *Proc Natl Acad Sci U S A* 96: 14553-8

Silver LL (2017) Fosfomycin: Mechanism and Resistance. *Cold Spring Harb Perspect Med* 7

Simunovic M, Manneville JB, Renard HF, Evergren E, Raghunathan K, Bhatia D, Kenworthy AK, Voth GA, Prost J, McMahon HT, Johannes L, Bassereau P, Callan-Jones A (2017) Friction Mediates Scission of Tubular Membranes Scaffolded by BAR Proteins. *Cell* 170: 172-184 e11

Smith MB, Karatekin E, Gohlke A, Mizuno H, Watanabe N, Vavylonis D (2011) Interactive, computer-assisted tracking of speckle trajectories in fluorescence

microscopy: application to actin polymerization and membrane fusion. *Biophys J* 101: 1794-804

Snead WT, Zeno WF, Kago G, Perkins RW, Richter JB, Zhao C, Lafer EM, Stachowiak JC (2019) BAR scaffolds drive membrane fission by crowding disordered domains. *J Cell Biol* 218: 664-682

Sohlenkamp C, Geiger O (2015) Bacterial membrane lipids: diversity in structures and pathways. *FEMS Microbiology Reviews* 40: 133-159

Spizizen J (1958) TRANSFORMATION OF BIOCHEMICALLY DEFICIENT STRAINS OF BACILLUS SUBTILIS BY DEOXYRIBONUCLEATE. *Proc Natl Acad Sci U S A* 44: 1072-8

Stahl E, Martin TG, Praetorius F, Dietz H (2014) Facile and scalable preparation of pure and dense DNA origami solutions. *Angew Chem Int Ed Engl* 53: 12735-40

Stepanyants N, Macdonald PJ, Francy CA, Mears JA, Qi X, Ramachandran R (2015) Cardiolipin's propensity for phase transition and its reorganization by dynamin-related protein 1 form a basis for mitochondrial membrane fission. *Mol Biol Cell* 26: 3104-16

Sterlini JM, Mandelstam J (1969) Commitment to sporulation in Bacillus subtilis and its relationship to development of actinomycin resistance. *Biochem J* 113: 29-37

Stragier P, Losick R (1996) Molecular genetics of sporulation in Bacillus subtilis. *Annu Rev Genet* 30: 297-41

Strahl H, Hamoen LW (2010) Membrane potential is important for bacterial cell division. *Proc Natl Acad Sci U S A* 107: 12281-6

Tan IS, Ramamurthi KS (2014) Spore formation in Bacillus subtilis. *Environ Microbiol Rep* 6: 212-25

Tarantino N, Tinevez JY, Crowell EF, Boisson B, Henriques R, Mhlanga M, Agou F, Israel A, Laplantine E (2014) TNF and IL-1 exhibit distinct ubiquitin requirements for inducing NEMO-IKK supramolecular structures. *J Cell Biol* 204: 231-45

Tinevez JY, Perry N, Schindelin J, Hoopes GM, Reynolds GD, Laplantine E, Bednarek SY, Shorte SL, Eliceiri KW (2017) TrackMate: An open and extensible platform for single-particle tracking. *Methods* 115: 80-90

Williams ND, Landajuela A, Kasula RK, Zhou W, Powell JT, Xi Z, Isaacs FJ, Berro J, Toomre D, Karatekin E, Lin C (2020) DNA-Origami-Based Fluorescence Brightness Standards for Convenient and Fast Protein Counting in Live Cells. *bioRxiv*: 2020.09.20.305359

Wong JY, Park CK, Seitz M, Israelachvili J (1999) Polymer-cushioned bilayers. II. An investigation of interaction forces and fusion using the surface forces apparatus. *Biophys J* 77: 1458-68

Wu Z, Bello OD, Thiyagarajan S, Auclair SM, Vennekate W, Krishnakumar SS, O'Shaughnessy B, Karatekin E (2017) Dilation of fusion pores by crowding of SNARE proteins. *Elife* 6

Yang C, Svitkina TM (2019) Ultrastructure and dynamics of the actin-myosin II cytoskeleton during mitochondrial fission. *Nat Cell Biol* 21: 603-613

Youngman PJ, Perkins JB, Losick R (1983) Genetic transposition and insertional mutagenesis in Bacillus subtilis with Streptococcus faecalis transposon Tn917. *Proc Natl Acad Sci U S A* 80: 2305-9

Zeigler DR, Pragai Z, Rodriguez S, Chevreux B, Muffler A, Albert T, Bai R, Wyss M, Perkins JB (2008) The origins of 168, W23, and other Bacillus subtilis legacy strains. *J Bacteriol* 190: 6983-95

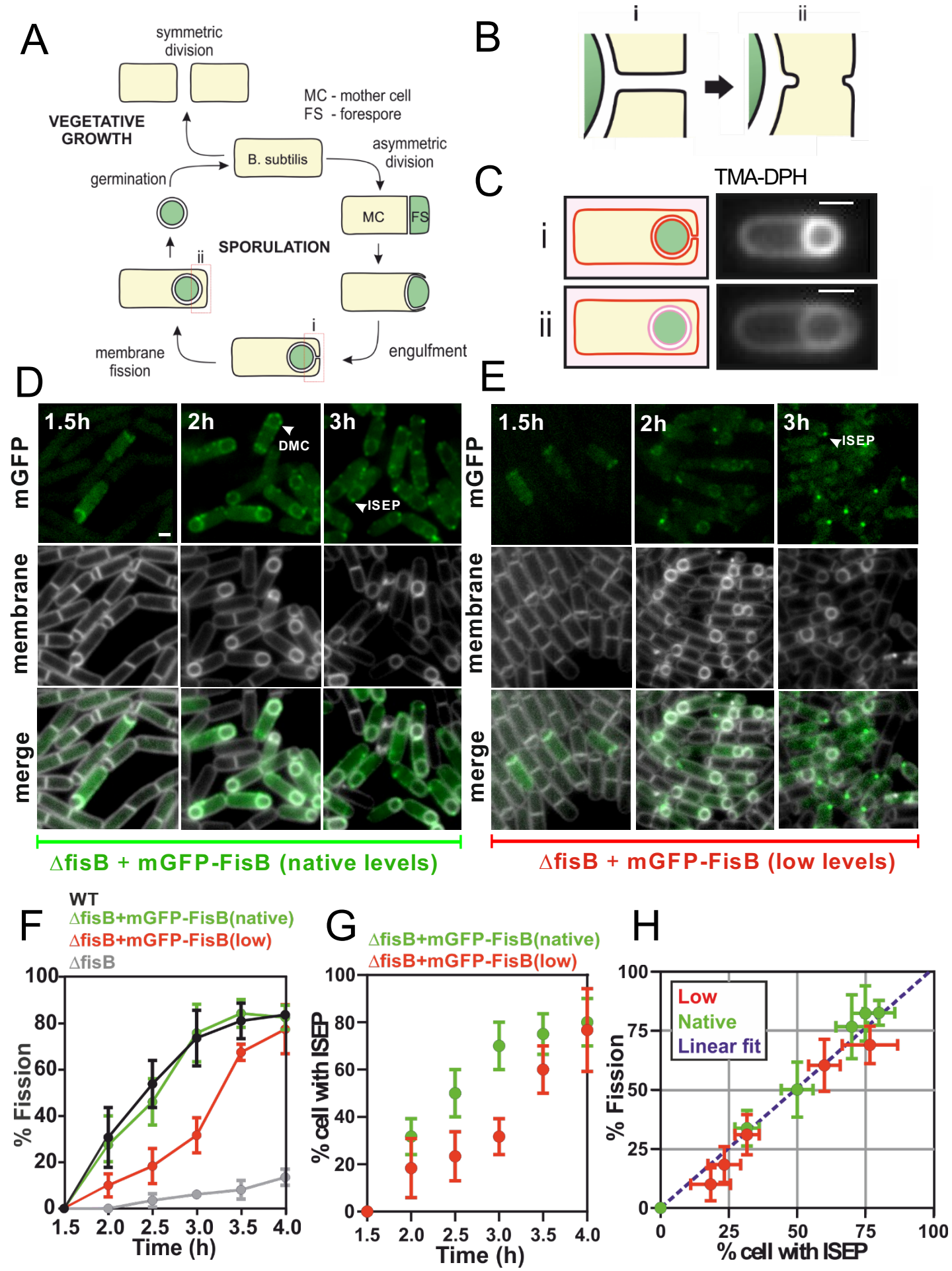
A
symmetric division
VEGETATIVE GROWTH
MC - mother cell
FS - forespore
B. subtilis
asymmetric division
germination
MC
FS
SPORULATION
ii
i
membrane fission
engulfment
B
i
ii
C
TMA-DPH
i
ii
D
1.5h
2h
3h
DMC
ISEP
mGFP
membrane
merge
ΔfisB + mGFP-FisB (native levels)
E
1.5h
2h
3h
ISEP
mGFP
membrane
merge
ΔfisB + mGFP-FisB (low levels)
F
WT
ΔfisB+mGFP-FisB(native)
ΔfisB+mGFP-FisB(low)
ΔfisB
% Fission
Time (h)
G
ΔfisB+mGFP-FisB(native)
ΔfisB+mGFP-FisB(low)
% cell with ISEP
Time (h)
H
Low
Native
Linear fit
% Fission
% cell with ISEP

FIGURE 1

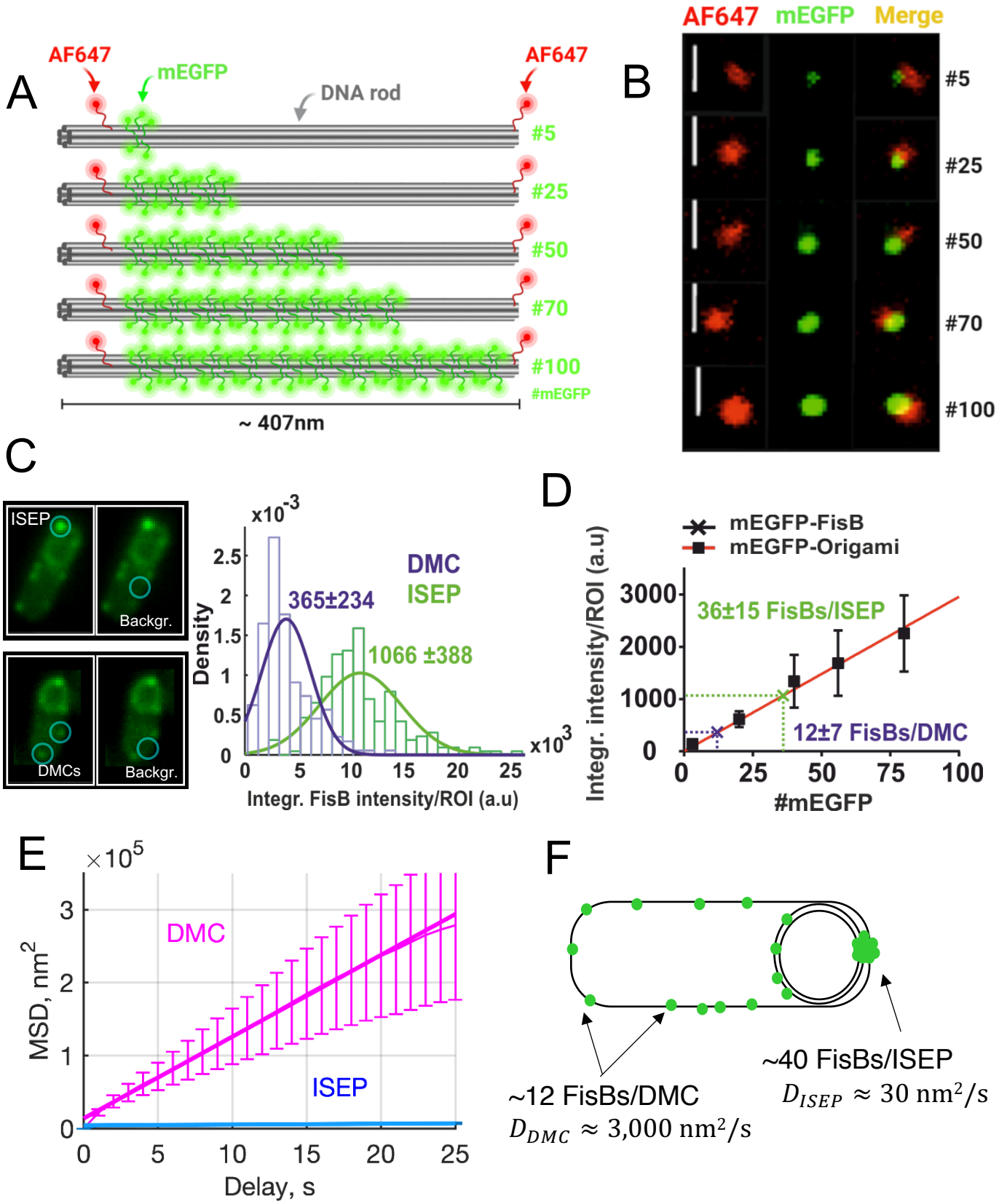
A
AF647
mEGFP
DNA rod
AF647
#5
#25
#50
#70
#100
#mEGFP
~ 407nm
B
AF647
mEGFP
Merge
#5
#25
#50
#70
#100
C
ISEP
Backgr.
DMCs
Backgr.
x10^-3
Density
DMC
ISEP
365±234
1066 ±388
x10^3
Integr. FisB intensity/ROI (a.u)
D
mEGFP-FisB
mEGFP-Origami
Integr. intensity/ROI (a.u)
36±15 FisBs/ISEP
12±7 FisBs/DMC
#mEGFP
E
×10^5
MSD, nm^2
DMC
ISEP
Delay, s
F
~12 FisBs/DMC
$D_{DMC} \approx 3{,}000\ \mathrm{nm}^2/\mathrm{s}$
~40 FisBs/ISEP
$D_{ISEP} \approx 30\ \mathrm{nm}^2/\mathrm{s}$

FIGURE 2

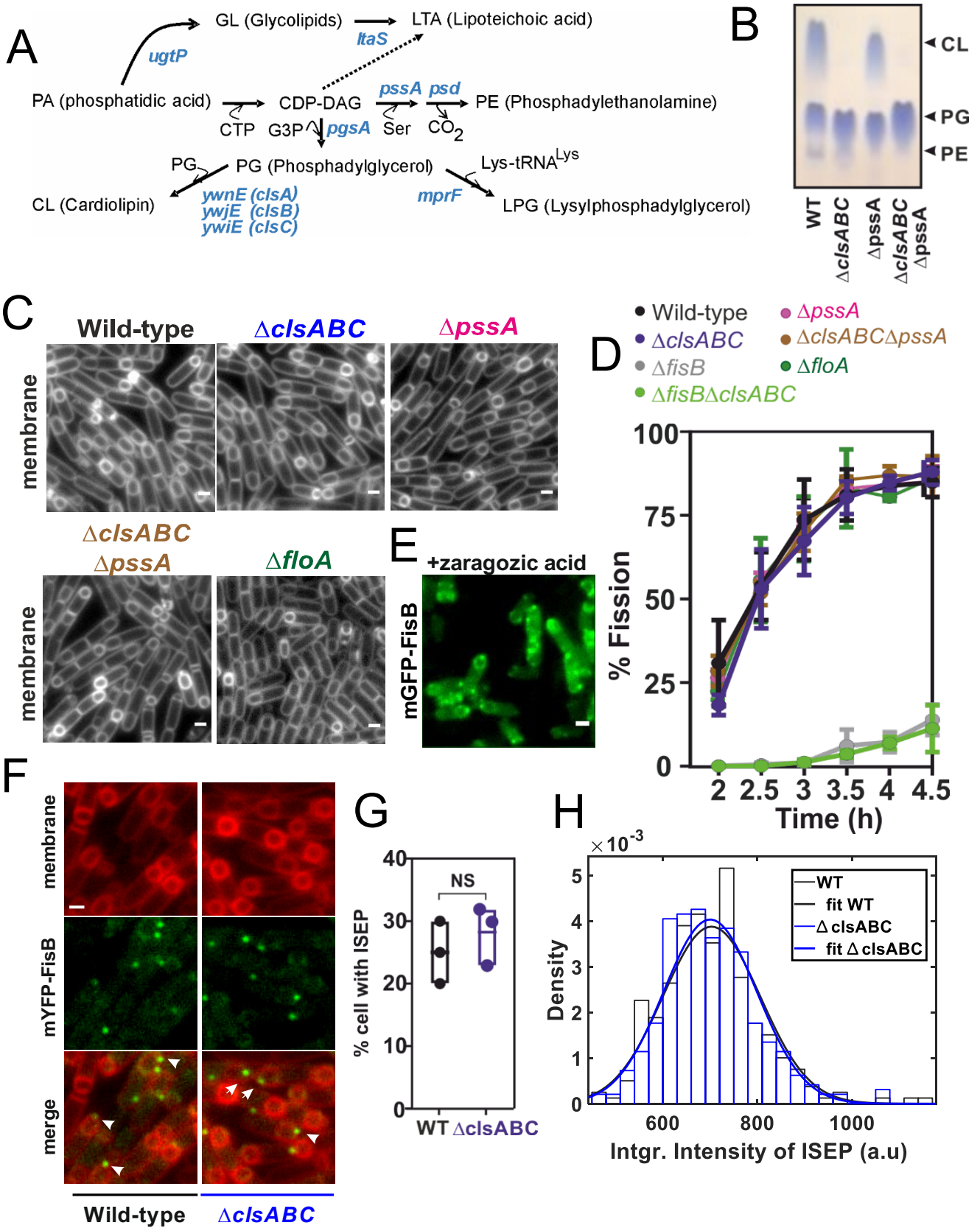
A
GL (Glycolipids)
LTA (Lipoteichoic acid)
ltaS
ugtP
PA (phosphatidic acid)
CDP-DAG
pssA psd
PE (Phosphadylethanolamine)
CTP G3P pgsA Ser CO2
PG
PG (Phosphadylglycerol)
Lys-tRNALys
CL (Cardiolipin)
ywnE (clsA)
ywjE (clsB)
ywiE (clsC)
mprF
LPG (Lysylphosphadylglycerol)
B
CL
PG
PE
WT
ΔclsABC
ΔpssA
ΔclsABC ΔpssA
C
Wild-type
ΔclsABC
ΔpssA
membrane
ΔclsABC ΔpssA
ΔfloA
E
+zaragozic acid
mGFP-FisB
D
Wild-type
ΔclsABC
ΔfisB
ΔfisBΔclsABC
ΔpssA
ΔclsABCΔpssA
ΔfloA
% Fission
Time (h)
F
membrane
mYFP-FisB
merge
Wild-type
ΔclsABC
G
% cell with ISEP
NS
WT ΔclsABC
H
×10-3
Density
WT
fit WT
Δ clsABC
fit Δ clsABC
Intgr. Intensity of ISEP (a.u)

FIGURE 3

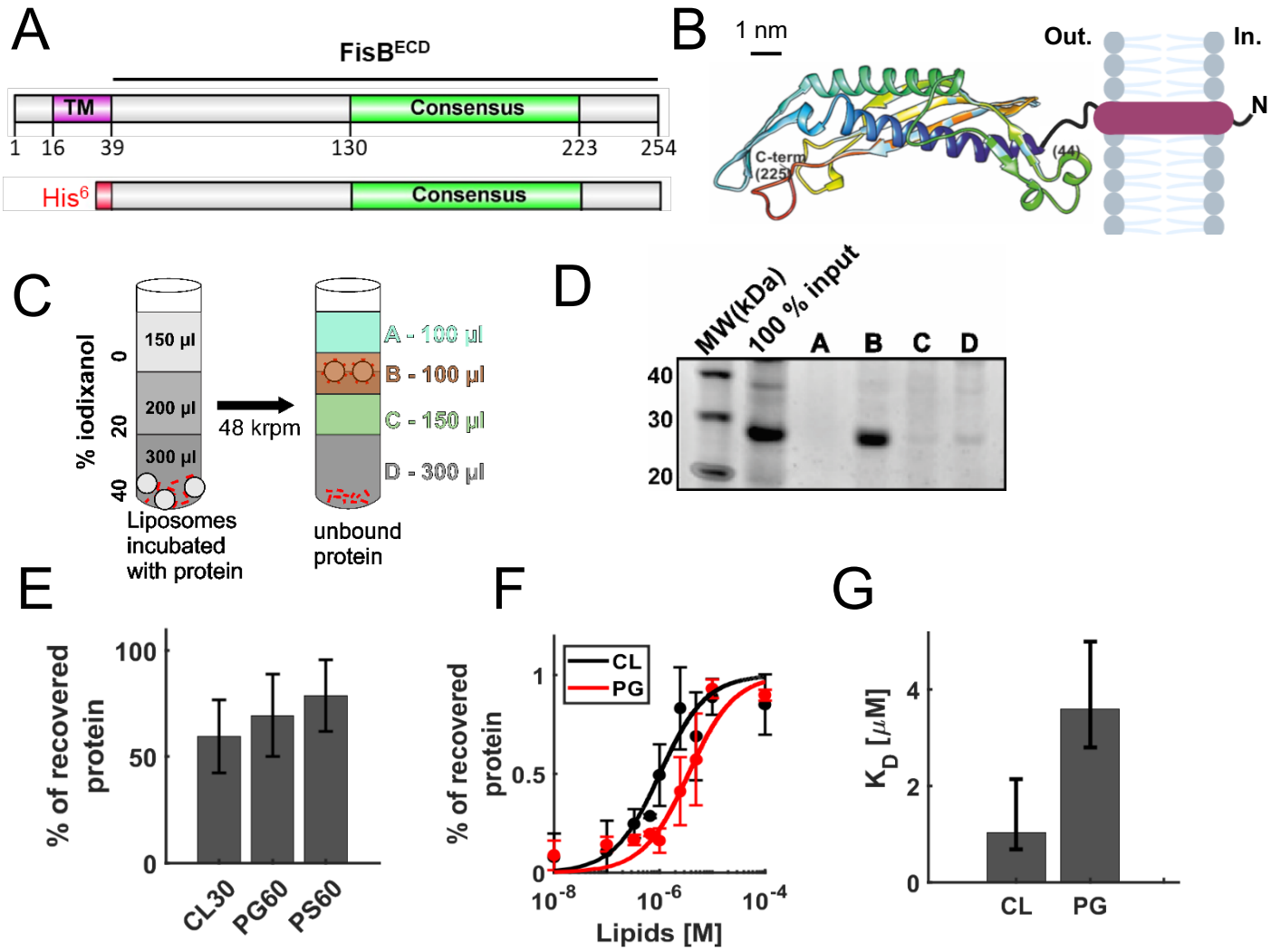
A
FisB^ECD
TM
Consensus
1
16
39
130
223
254
His6
Consensus
B
1 nm
Out.
In.
N
C-term
(225)
(44)
C
% iodixanol
0
20
40
150 µl
200 µl
300 µl
48 krpm
A - 100 µl
B - 100 µl
C - 150 µl
D - 300 µl
Liposomes
incubated
with protein
unbound
protein
D
MW(kDa)
100 % input
A
B
C
D
40
30
20
E
% of recovered
protein
100
50
0
CL30
PG60
PS60
F
% of recovered
protein
CL
PG
1
0.5
0
10^-8
10^-6
10^-4
Lipids [M]
G
K_D [µM]
4
2
0
CL
PG

FIGURE 4

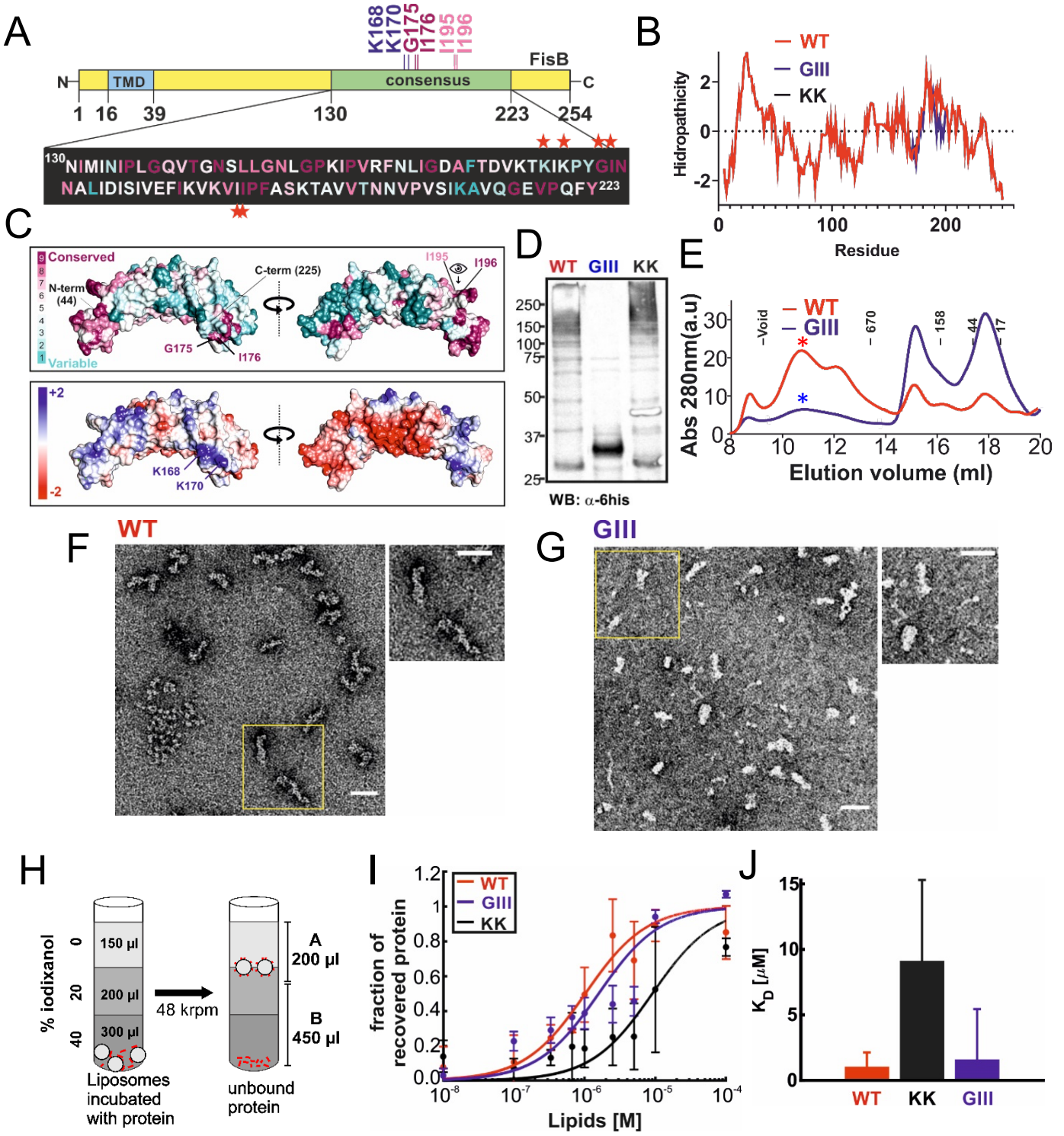
A
K168
K170
G175
I176
I195
I196
FisB
N
TMD
consensus
C
1 16 39 130 223 254
130NIMINIPLGQVTGNSLLGNLGPKIPVRFNLIGDAFTDVKTKIKPYGIN
NALIDISIVEFIKVKVIIPFASKTAVVTNNVPVSIKAVQGEVPQFY223
B
WT
GIII
KK
Hidropathicity
Residue
C
Conserved
Variable
N-term (44)
C-term (225)
G175
I176
I195
I196
+2
-2
K168
K170
D
WT GIII KK
250
150
100
75
50
37
25
WB: α-6his
E
WT
GIII
Abs 280nm(a.u)
Elution volume (ml)
Void
670
158
44
17
F
WT
G
GIII
H
% iodixanol
0
20
40
150 µl
200 µl
300 µl
48 krpm
Liposomes incubated with protein
unbound protein
A
200 µl
B
450 µl
I
WT
GIII
KK
fraction of recovered protein
Lipids [M]
J
K_D [µM]
WT
KK
GIII

FIGURE 5

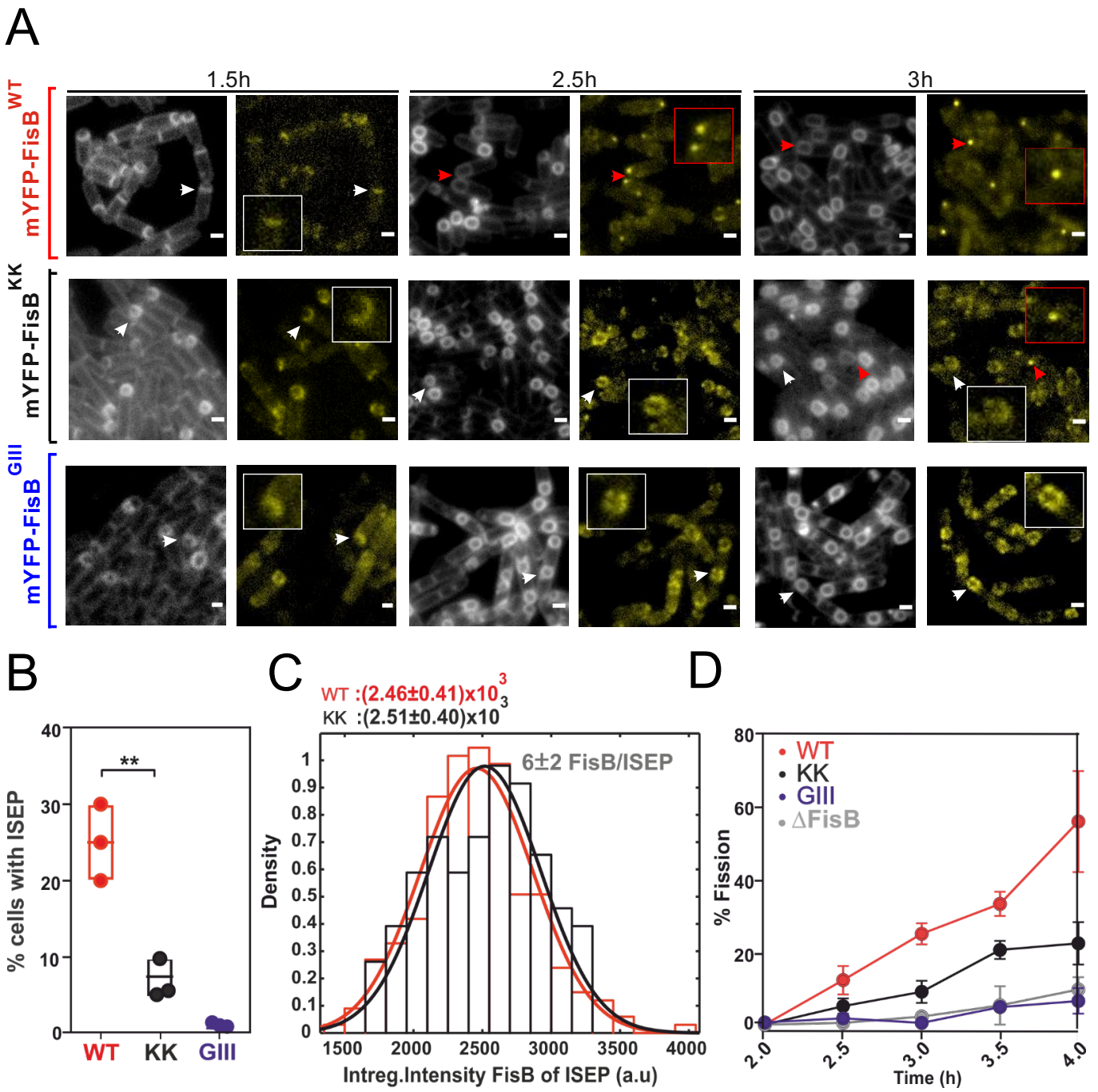
A
1.5h
2.5h
3h
mYFP-FisB WT
mYFP-FisB KK
mYFP-FisB GIII
B
% cells with ISEP
**
WT
KK
GIII
C
WT :(2.46±0.41)x10^3
KK :(2.51±0.40)x10^3
6±2 FisB/ISEP
Density
Intreg.Intensity FisB of ISEP (a.u)
D
WT
KK
GIII
ΔFisB
% Fission
Time (h)

FIGURE 6

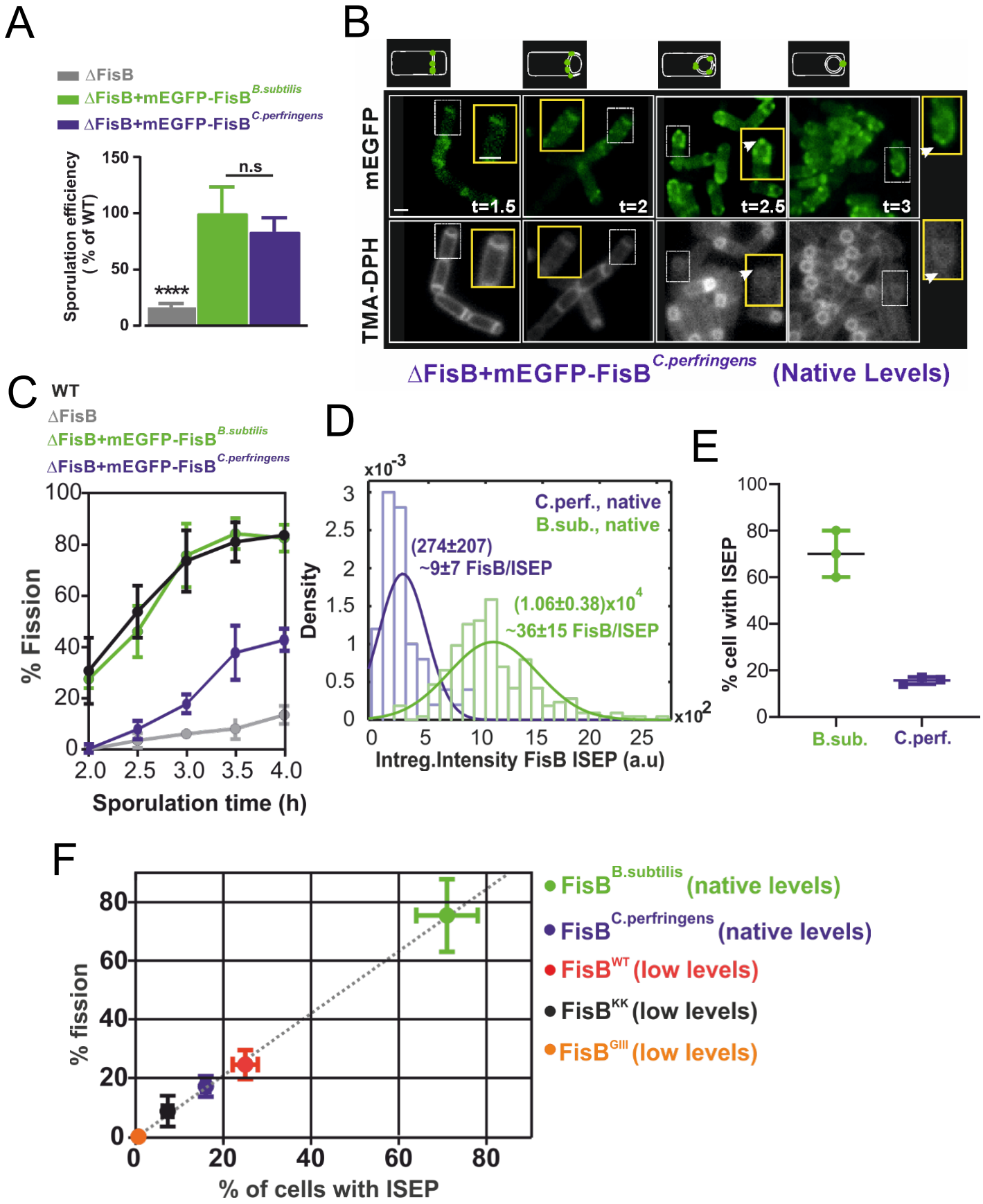
A
ΔFisB
ΔFisB+mEGFP-FisB B.subtilis
ΔFisB+mEGFP-FisB C.perfringens
Sporulation efficiency (% of WT)
150
100
50
0
n.s
****
B
mEGFP
TMA-DPH
t=1.5
t=2
t=2.5
t=3
ΔFisB+mEGFP-FisB C.perfringens (Native Levels)
C
WT
ΔFisB
ΔFisB+mEGFP-FisB B.subtilis
ΔFisB+mEGFP-FisB C.perfringens
% Fission
Sporulation time (h)
D
x10-3
C.perf., native
B.sub., native
(274±207)
~9±7 FisB/ISEP
(1.06±0.38)x10 4
~36±15 FisB/ISEP
Density
Intreg.Intensity FisB ISEP (a.u)
x10 2
E
% cell with ISEP
B.sub.
C.perf.
F
% fission
% of cells with ISEP
FisB B.subtilis (native levels)
FisB C.perfringens (native levels)
FisB WT (low levels)
FisB KK (low levels)
FisB GIII (low levels)

FIGURE 7

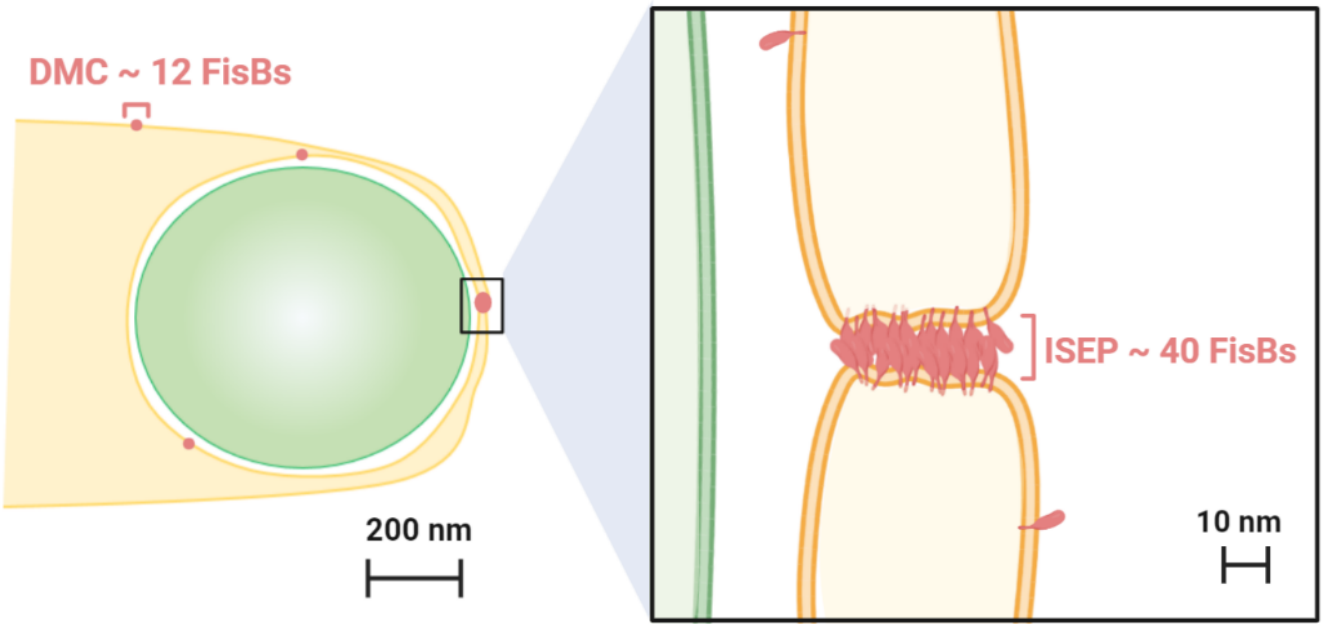

FIGURE 8